Photo- and Electrochromism of Polyoxometalates and Related Materials

Toshihiro Yamase

Research Laboratory of Resources Utilization, Tokyo Institute of Technology, 4259 Nagatsuta, Midori-ku, Yokohama 226, Japan

Received April 1, 1997 (Revised Manuscript Received October 17, 1997)

Contents

Toshihiro Yamase was born in Kanazawa, Japan, in 1943. He received a B.S. in 1965 from Nagoya Institute of Technology and obtained a Ph.D. in 1970 for his studies of the sensitized photolysis of dithiocarbamates from Tokyo Institute of Technology with Eiichi Inoue. He became a research associate with Tsuneo Ikawa in 1971 for his work on the dye-sensitized photolysis of diazonium salts. After postdoctoral work on dye sensitization on the semiconductor electrode at Fritz-Haber-Institut der Max-Planck-Gesellschaft, with Heinz Gerischer from 1976 to 1977, he joined Tokyo Institute of Technology again in 1977 and became full Professor in 1989. His research efforts have been in the structure, photochemistry, and biological activity of polyoxometalates. His research interest is molecular devices based on polyoxometalates.

I. Introduction

A. Historical Background

The photochemistry of polyoxometalates is of great interest to inorganic chemists. More than 80 years ago, it was found that the α-Keggin tungstate $H_3[PW_{12}O_{40}]$ was reduced photochemically to yield a blue-colored species which was reoxidized by air and by various other oxidizing agents such as Fe^{3+}, $AgNO_3$, and H_2O_2.[1,2] The photoredox reactions of $H_4[SiW_{12}O_{40}]$ and $H_3[PW_{12}O_{40}]$ proceeded effectively in the presence of primary and secondary alcohols, their ethers and aldehydes, and proteins, but less effectively in the presence of tertiary alcohols, ketones, esters, the fatty acids above formic acid, and simple amines.[3,4] The basic photoredox reaction involving ethanol is illustrated by eq 1.

$$2H_3PW_{12}O_{40} + H_3CCH_2OH \xrightarrow{h\nu} 2H_4PW_{12}O_{40} + H_3CCHO \quad (1)$$

$$2H_4PW_{12}O_{40} + {}^1/_2O_2 \rightarrow 2H_3PW_{12}O_{40} + H_2O \quad (2)$$

In this reaction, one molecule of ethanol photochemically reduces two molecules of $H_3PW_{12}O_{40}$ and is itself oxidized to acetaldehyde. In the presence of air, the thermal oxidation of the reduced species takes place at room temperature (eq 2). The reduced polyoxometalates, which are the so-called "heteropoly blues", have been used for the colorimetric analysis of the elements P, Si, As, and Ge and for the determination of uric acid, sugar, and other biological compounds.[5,6] Piperidinium metavanadate ($[C_5H_{10}NH_2][VO_3]$) also undergoes photoinduced coloration from white to black, followed by a reversible color change in the presence of oxidizing agents. However, ammonium metavanadates ($[NH_4][VO_3]$) exhibits no photoinduced coloration.[7] The early photoredox reactions of the α-Keggin polyoxometalates $H_4[SiW_{12}O_{40}]$ and $H_3[PW_{12}O_{40}]$ were carried out in the presence of

S0009-2665(96)00404-9 CCC: $30.00
Published on Web 01/07/1998

photographic paper; however, the limited number of the structurally well-characterized compounds available for study delayed the development of modern cluster−compound photochemistry until the discovery of photochromism in alkylammonium polyoxomolybdate solids.[8,9]

A photochromic or electrochromic material is one whose light-absorbing properties are altered upon optical excitation or reduction under the influence of an externally applied electric field, respectively. The induced coloration remains even after the excitation source has been removed. These materials are of technological interest because they return to their original state either thermally, upon irradiation with light of a frequency corresponding to the induced absorption, or electrochemically, upon reversing the polarity of the externally applied electric field. Thus, photochromic and electrochromic materials behave in a reversible manner. Polyoxometalates exhibit significant photo- and electrochromism which makes them suitable as nanocomposite molecular devices and as models for probing the physical properties of infinite metal oxides.

B. Scope and Limitations

Since the metal ions in the oxidized polyoxometalates have d^0 electronic configurations, the only absorption band which occurs in the UV−vis range of the electronic spectra is due to the oxygen-to-metal (O→M) ligand-to-metal charge transfer (LMCT). Upon irradiation, electrons are promoted from the low-energy electronic states, which are mainly comprised of oxygen 2p orbitals (the valence band in the band model), to the high-energy electronic states, which are mainly comprised of metal d orbitals (the conduction band in the band model). The fundamental transitions in polyoxometalate lattices are depicted schematically in Figure 1. In the polyoxometalates containing heteroatoms, and especially in mixed metal polyoxometalates, the charge carriers which are created by the light or electric field may be trapped in electron traps and hole traps. These traps provide states of localized energy in the O→M LMCT energy gap due to the heteroatoms or counter cations which correspond to impurities or lattice defects in the band model. If the trap depth, ΔE, is large compared to kT, the probability for thermal escape from the trap will be negligibly small and metastable situation will exist. The trapped carriers can be released by thermal or optical stimulation. In the case of thermal stimulation, the irradiated polyoxometalate is heated until the energy barrier ΔE can be overcome. The trapped electron (or hole) then can escape from the trap and nonradiatively recombine with the trapped hole (or electron). Under optical stimulation, the energy of an incident photon is used to overcome ΔE. The relaxation processes of the O→M LMCT excitation energy include both the nonradiative recombination of electrons and holes within the energy gap and the intramolecular energy transfer leading to a charge-transfer emission. This intramolecular energy transfer corresponds to the O→M LMCT energy gap and occurs via radiative recombination and sensitized emission from the

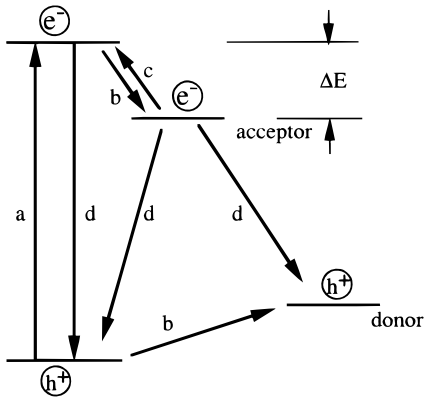

Figure 1. Simple model showing the electronic transitions in the polyoxometalates containing electron donor and acceptor: (a) generation of charge carriers; (b) electron and hole trapping; (c) electron release due to stimulation; (d) recombination between electron and hole. Electrons are e^-, and holes are h^+.

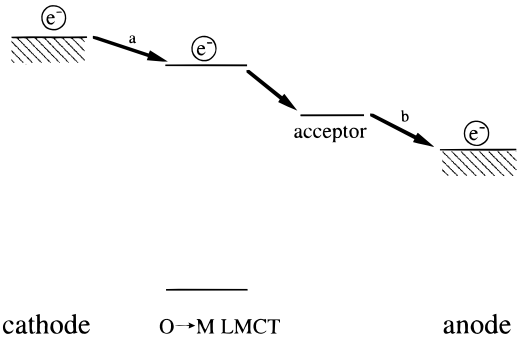

Figure 2. Energy scheme for the electrochromism of polyoxometalates: (a) electrochemical reduction; (b) electrochemical oxidation.

heteroatoms or cations. If several energy levels based on the heteroatoms or counter cations act as energy acceptors within the O→M LMCT energy gap, the energy transfer occurs from the O→M LMCT states to these levels, followed by the nonradiative or radiative deactivation of the excitation energy. It should be noted that the O→M LMCT states also can be generated by the application of very high electric fields to the polyoxometalate solids, as demonstrated by the observation of electroluminescence.[10]

If an external electric field with a potential more negative than the energy levels of the vacant orbitals involved in the O→M LMCT transition is applied to a polyoxometalate on the electrode surface, an electrochemical reduction occurs via the injection of electrons from the electrode into the vacant levels of the polyoxometalate, as shown in Figure 2. Electrons injected into the high-energy levels also may be trapped by electron traps, in a process analogous to that which occurs during LMCT photoexcitation of the polyoxometalates. These electrons are returned to the electrode by electrochemical oxidation at an electrode potential more positive than the energy levels for the d^1 electron states.

The d^1 electrons in the O→M LMCT states facilitate the absorption of visible light via intervalence charge transfer among metal centers and d−d transitions. The same type of transition may be possible

for the d^1 electron captured by the electron traps, too. In addition, to searching for new photosensitive polyoxometalates with the potential for having practical application, there is now a need to elucidate the fundamental photo- and electrochemical coloration processes by studying electron transfer within the polyoxometalate lattices in conjunction with their crystal structures. So far, few polyoxometalates exhibit a perfect reversibility of coloration. The irreversibility of the color change arises from as yet uncharacterized side reactions during both the coloration and decoloration of the polyoxometalates.

In this paper the results of experiments dealing with both electron transfer and energy transfer within polyoxometalate and related metal oxide solids are illustrated and discussed. I place particular emphasis on the structural characterization of both oxidized and reduced polyoxometalates in connection with the mechanistic feature of the coloration. The photoredox reactions of the polyoxometalates with organic substances, which yield heteropoly blues in solution,[11−15] is not included here. Furthermore, only crystallographically well-characterized heteropoly blues which are prepared by photoredox reactions in solutions are addressed. However, photoinduced self-assembly reactions involving coloration will be described, since they define the feasibility of a novel method to prepare practically useful nanocomposite materials.

II. Photochromism and Electrochromism of Metal Oxides

A. Photoinduced Coloration of Metal Oxides Due to Impurity Effects

Many metal oxides including aluminum, titanium, vanadium, niobium, molybdenum, and tungsten oxides are photochromic when they contain impurities, or dopants. This coloration has been interpreted on the basis of electron trapping at appropriate lattice sites within the crystals, as shown in Figure 1, where the O→M LMCT transition corresponds to the transition between the valence and conduction bands for the infinite metal−oxide lattice.[16−19] Table 1 shows coloring behavior of the metal oxides with dopants.

Sodalite, which has the chemical formula $Na_6Al_6Si_6O_{24}\cdot 2NaX$ (X = halogen), is colored by UV (photochromic) and by electron beam (cathodochromic) irradiation due to an electron (the color center) which is trapped at a halogen vacancy.[20−34] Both sodium ion vacancies and O^{2-} ion impurities in the halogen sites have been proposed as hole-trapping sites. The induced coloration is bleached from the material upon exposing it to visible light or heat, due to the recombination of the trapped electrons and holes. The sodalite materials are prepared by solid-state sintering (700−1050 °C) of a mixture of Na_2CO_3, Al_2O_3, SiO_2, NaCl, and Na_2SO_4 in air. The achievable contrast ratio, decay time, optical erasability, and color of the materials change considerably depending on number of sulfate radicals incorporated. The composition of $Na_6Al_6Si_6O_{24}\cdot 1.2NaCl\cdot 0.4Na_2SO_4$ shows the best compromise among these properties. The peak wavelength of this compound's induced absorption spectrum is 553 nm, and its thermal decay time at room temperature is about 30 min.[35]

When Mn (0.005%) is incorporated into Fe (0.05%)-doped $LiNbO_3$, photochromic behavior involving the photoreversible conversion of Fe^{3+} to Fe^{2+} is observed with the absorption peaking around 450 nm.[36−39] This process is considered to be useful for controlling holographic storage sensitivity.[40−42]

TiO_2 becomes photochromic when small amounts (0.01−0.5%) of some metals (Fe, Ni, Cu, Cr, Co, Mn, and certain rare earth metals) or their oxides are added to it, if the impurity is adsorbed onto the surface of the TiO_2 in a rutile form.[43] On irradiation, the stable, low-valent impurity ions on the TiO_2 surface are oxidized to a higher, colored valency state.[44] Upon cessation of irradiation, the high valence form of the ions reverts to the low valence form within minutes to weeks at temperatures <100 °C. The presence of oxygen and moisture appears to be essential to this photolytic reaction.

When Fe- and Mo-doped $SrTiO_3$ or TiO_2 compounds are irradiated with light in the 390−430 nm region, broad visible absorption bands appear due to the formation of Fe^{4+} and Mo^{5+} via electron transfer from Fe^{3+} to Mo^{6+}.[44−46] This process does not depend on the surface effect. At 300 K, thermal bleaching of the photoinduced colored state occurs within several minutes for the Fe/Mo-doped $SrTiO_3$ and within less than a second for the Fe/Mo-doped TiO_2.

Freshly evaporated films of WO_3, MoO_3, and V_2O_5, in which the metal oxides exist in well-defined oxygen-deficient phases, can be colored to a deep blue by irradiating them with UV light for several hours. The colored films then can be bleached by heating them in an oxidizing atmosphere at a temperature near 300 °C. Once the films are oxidized, however, they do not undergo further coloration.[47]

Calcium, strontium, and barium tungstates and their solid solutions color remarkably on exposure to UV light when doped with a small amount of bismuth. These tungstates turn to their original white color by thermal fading or optical bleaching.[48] The intensity of the tungstates' UV-induced coloration depends on their Bi content and preparation tem-

Table 1. Coloring Behavior of Metal Oxides with Dopants

host metal oxide	dopant	UV-induced coloring	color before exposure
Sodalite $Na_6Al_6Si_6O_{24}\cdot 2NaX$ (X = halogen)	halogen-ion vacancy	magenta	white
$LiNbO_3$	Fe, Mo	brown	pale yellow
TiO_2	Fe_2O_3 or $FeSO_4$	brown	white
$StTiO_3$ or TiO_2	Fe, Mo	brown	white
WO_3, MoO_3, V_2O_5	oxygen vacancy	blue	pale yellow
$(AE)WO_4$ (AE = alkaline earth)	Bi	purple, green, pink	white

perature. Bi contents higher than 0.1 mol % and preparation temperatures higher than 1250 °C give strong coloration. The fading rate of the UV-induced color is 30 min at 230 °C and also is increased by visible light exposure.

B. Electrochromism

1. WO_3

WO_3 is one of the most well-known electrochromic materials,[19,47,49−53] WO_3-based electrochromic cells are composed of a front glass substrate, a display electrode, an electrolyte, a reflector/counter electrode, and a back cover glass substrate, as shown in Figure 3. The inside of the cover glass is coated with an ITO (In_2O_3/SnO_2) film. The WO_3 film is usually prepared by vacuum evaporation, in which the oxides are deposited onto the conducting ITO glass substrates. These films appear uniform by optical microscopy at ×100 magnification, and X-ray and electron diffraction show that they are amorphous. The WO_3 film consists of nonstoichiometric oxide phases containing a large number of oxygen ion vacancies, which results in a partial structural change from corner-sharing to edge-sharing WO_6 octahedra. It has been proposed that the WO_3 films consist of trimeric W_3O_9 molecules bound weakly to each other through water bridges, hydrogen bonding, and van der Waal's forces. The film's high solubility is attributed to this microstructure. Films which are subjected to ion bombardment show decreased dissolution rates as well as decreased electrochromism and, while still amorphous, are believed to have a random network structure rather than a molecular microstructure.[54] In general, the electrocoloration in the WO_3 film results from the formation of a tungsten bronze (M_xWO_3, $x = 0-1$), as denoted by eq 3:

$$WO_3\ (\text{colorless}) + xM^+ + xe^- \rightarrow M_xWO_3\ (\text{blue}) \quad (3)$$

M can be H, Li, or Na, and the formation of the tungsten bronze is caused by the double injection of M^+ ions and electrons into the WO_3. The blue color of the tungsten bronze is attributed to the intervalence charge transfer of electrons between W^{6+} and W^{5+}.

Water plays an important role in the coloration and bleaching of the WO_3 film.[55−59] Water adsorbed on the film from the ambient air after ventilation of the vacuum evaporation chamber causes an initial fast electrochromic reaction and then gradually hydroxylates and hydrolizes the WO_3, which shifts the potential of the cathodic reaction to a more negative voltage. The hydroxylated film loses its electrochromic coloration reaction to a more negative voltage. The hydroxylated film loses its electrochromic coloration density at the same applied voltage as before.[60−62] In highly humid air, the tungstates $WO_3 \cdot H_2O$ and $H_2WO_4 \cdot H_2O$ are formed and cause remarkable deterioration of the electrochromic activity of the film.

The kinetics of the electrochromic process has been studied, as has the stability of different WO_3 electrodes, including evaporated film electrodes, electrodes obtained by anodic oxidation of W, polycrystalline electrodes, and single-crystal electrodes.[63] The impedances of the WO_3/H_2SO_4(aq) interface at different frequencies also have been compared for the evaporated film and anodic oxide electrodes. The results indicate that the electrochromic reaction at the WO_3 anodic film is much faster than at the evaporated film electrode by about 2−3 orders of magnitude. The difference in these reaction rates reflects the different rates of H^+ diffusion in the films, which is caused by variations in the film porosities and water content. Furthermore, both the solvent and the nature of the cation affect the kinetics of the WO_3 species' electrochromic processes and the stability of the amorphous films.

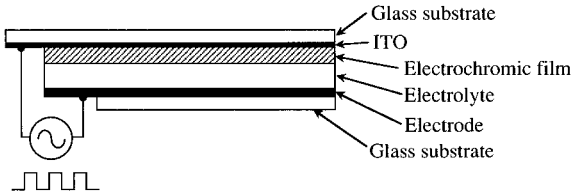

Figure 3. Schematic structure of a simple electrochromic cell based on amorphous WO_3 film.

Unfortunately, the WO_3 electrochromic display exhibits a short device life, and this limits its commercial potential. Degradation of the WO_3 in the electrochromic cell is caused by film dissolution on the shelf and by erosion during cycling. Aqueous acid cell show superior response speed; however, the presence of water shortens their life span through WO_3 dissolution. Nevertheless, the incorporation of some water into the WO_3 film is necessary in order to obtain electrochromic coloration. The electrochromic reliability and response time of an amorphous WO_3-based electrochromic cell is dependent not only by the WO_3 film but also on the electrolyte and counter electrode. A lifetime of $>10^7$ cycles and response times of 100 ms were obtained for the $WO_3/LiClO_4$−propylene carbonate electrochromic display at a charge density of 6 mC/cm^2 at 25 °C.[64] Transmissive solid-state electrochromic devices based on the WO_3/Li−polymer (PMMA) electrolyte/V_2O_5 system have been optimized for potential large-area window applications, and the best layer thickness combination was found to be 8000 Å WO_3 and 1150 Å V_2O_5.[65] Long-term operation, that is, a cycling lifetime of more than 5×10^5 and a static lifetime of 10−40 years at an operating temperature of −20 to 85 °C, is a critical requirement in this technology, especially if device lifetimes in excess of 20 years are to be achieved.[66]

2. Other Metal Oxides

Iridium oxide films deposited on an iridium electrode by anodic oxidation exhibit electrochromic properties with a high response time of ∼50 ms, as denoted by the color change during the redox process in eq 4.[67−69]

$$Ir(OH)_n\ (\text{colorless}) \rightarrow IrO_x(OH)_{n-x}\ (\text{dark blue}) + xH^+ + xe^- \quad (4)$$

Although long-term stabilization of this system against corrosion is obtained in 0.5 M Na_2SO_4 at pH 3.5, degradation of the bleaching response time occurs under these conditions. The electrochromic iridium oxide films also can be prepared by either sputtering or thermal oxidation.[70,71] However, the reflectivity of the redox reaction will have to be increased and made more efficient if these systems are to find practical application.

Oxides of nickel and vanadium are electrochromic materials which exhibit various color changes during their redox process.[72−74] Nickel oxide films which are grown by a variety of vacuum technologies from NiO powder targets usually have a composition of NiO_z with $z > 1$. After electrochemical formatting, the optically active film has a composition of $Li_xNi_{1-x}O$, where x is about 0.3−0.5. $Li_xNi_{1-x}O$ is anodically colored and thus complements cathodically colored WO_3. The actual electrochromic process takes place between $Li_{x+y}Ni_{1-x}O$ and colored $Li_{x+y-\delta}Ni_{1-x}O$ with y being close to δ. The typical optical transmission range of this material is from 20 to 30% at 550 nm. Cyclic voltammograms and long-term cycling have been tested over 10^3 cycles.[75]

Vanadium oxide (V_2O_5) films which are deposited by rf reactive sputtering at high oxygen flow show good electrochromic performance. These films are cathodically colored at wavelengths of >500 nm by charges inserted according to the reaction $V_2O_5 + xLi^+ + xe^- \rightarrow Li_xV_2O_5$ at up to −25 mC/cm^2.[76] The films have an amorphous microstructure and a high hydrogen content. The hydrogen is present either as O−H groups or as water molecules. When the films are deposited at low oxygen flow, there is a resultant decrease in vanadium oxide content, and the films are not electrochromic.

III. Photochromism of Polyoxometalate Solids

A. Alkylammonium Polyoxomolybdates

Alkylammonium polyoxomolybdates are discrete molecules which can be differentiated from infinite metal oxides and are photosensitive both as solids and in solution. When the primary, secondary, and tertiary ammonium polyoxomolybdates are irradiated with UV light at wavelengths corresponding to the O→Mo LMCT transition (λ<400 nm), the white crystals become reddish brown or violet, signaling the formation of $Mo^VO_5(OH)$.[8,77−79] The colored polyoxomolybdates return to their original white color in the presence of oxygen in the dark, but the colored monomethyl- and monoethylammonium polyoxomolybdate salts do not return. This color change can be repeated many times. A French group also has demonstrated that secondary ammonium salts of polyoxomolybdates are photochromic.[9,80] Table 2 contains a complete list of the photosensitive alkylammonium polyoxomolybdate solids, while Figure 4 shows examples of the structures of the anionic portion of these compounds ($[NH_3Pr^i]_6[Mo_7O_{24}]\cdot 3H_2O$,[81] $[NH_3Pr]_6[Mo_7O_{24}]\cdot 3H_2O$,[81] $[NH_3Pr^i]_6[Mo_8O_{26}(OH)_2]\cdot 2H_2O$,[82] $[NH_3Me]_8[Mo_8O_{26}(MoO_4)_2]\cdot 2H_2O$,[83] and $[NH_2Me_2]_4[Mo_6O_{20}]\cdot 2H_2O$.[84] The most photosensitive compound, $[NH_2Me_2]_4[Mo_6O_{20}]\cdot 2H_2O$, contains a

Table 2. Photosensitive Alkylammonium Polyoxomolybdate Solids[73]

polyoxomolybdates	space group[a]	λ_{max} of colored state (nm)	rel rate of color-ation	rel rate of fading
$[NH_3Pr^i]_6[Mo_7O_{24}]\cdot 3H_2O$[81]	$P2/n$ (4)	510	1	2
$[NH_3Pr]_6[Mo_7O_{24}]\cdot 3H_2O$[81]	$P\bar{1}$ (2)	490	1	4
$[NH_3Pr^i]_6[Mo_8O_{26}(OH)_2]\cdot 2H_2O$[82]	$P\bar{1}$ (1)	480	2	1
$[NH_3Me]_8[Mo_8O_{26}(MoO_4)_2]\cdot 2H_2O$[83]	$P2_1/n$ (2)	480	4	
$[NH_2Me_2]_4[Mo_6O_{20}]\cdot 2H_2O$[84]	$P2_1$ (2)	470	>7	8

[a] The number of molecules in unit cell is indicated in parentheses.

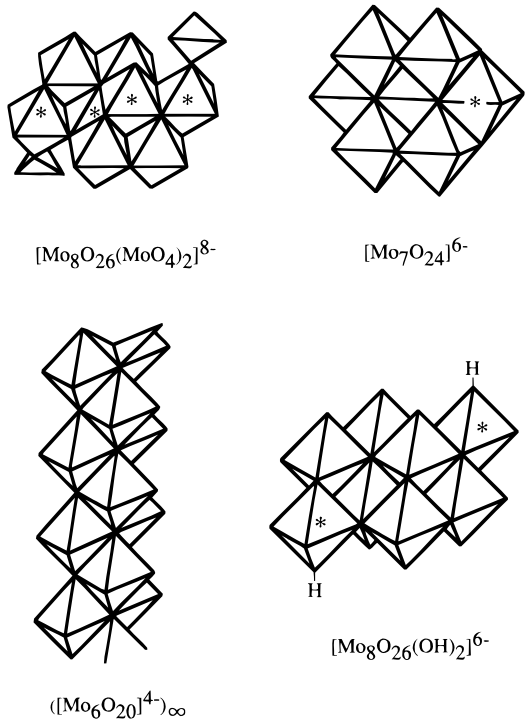

Figure 4. Structures of anions of the photosensitive alkylammonium-polyoxomolybdates. An asterisk (*) indicates the photoreducible MoO_6 site associated with the transfer of the hydrogen-bonded alkylammonium proton. The photoreducible site for fibrous crystals of $[NH_2Me_2]_4[Mo_6O_{20}]\cdot 2H_2O$ is not determined yet, because of difficulty in the preparation of single crystals with a moderate size.

$\{[Mo_6O_{20}]^{4-}\}_\infty$.[84] Other known isopolyoxomolybdate infinite chains include $\{[Mo_8O_{26}(O)]^{6-}\}_\infty$ and $\{[Mo_8O_{26}(MoO_4)]^{6-}\}_\infty$ in the crystals of $[NH_4]_6[Mo_8O_{27}]\cdot 4H_2O$[85] and $[NH_4]_6[Mo_8O_{26}(MoO_4)]\cdot 5H_2O$,[86] respectively. The former, in which the Mo_8O_{26} moieties are arranged parallel to each other, is regarded as a condensed version of the discrete $[Mo_8O_{26}(OH)_2]^{6-}$ anion found in the photosensitive compound $[NH_3Pr^i]_6[Mo_8O_{26}(OH)_2]\cdot 2H_2O$.[82] Likewise, $[Mo_8O_{26}(MoO_4)_2]^{8-}$ in which two adjacent Mo_8O_{26} moieties are linked by a MoO_4 tetrahedron to form an infinite zigzag chain, is regarded as a condensed analog of the discrete $[Mo_8O_{26}(MoO_4)_2]^{8-}$ anion from the photosensitive compound $[NH_3Me]_8[Mo_8O_{26}(MoO_4)_2]\cdot 2H_2O$.[83] Following solid-state irradiation of the alkylammonium polyoxomolybdates, the colored, metastable state is characterized by single-crystal ESR spectroscopy.[79,87−89] From this it has been deduced that photoexcitation

of the alkylammonium polyoxomolybdate's O→M LMCT bands induces transfer of a proton from a hydrogen-bonded alkylammonium nitrogen to a bridging oxygen atom at the photoreducible site in the edge-shared MoO_6 octahedral lattice. This is followed by the interaction of the d^1 electron with the proton which was transferred to the oxygen atom. Simultaneously, the hole left at the oxygen atom as a result of the O→Mo LMCT transition interacts with nonbonding electrons on the amino nitrogen atom to form a charge-transfer complex (**i**). Equation 5 denotes the environment of the photoreducible MoO_6 site and the subsequent formation of the charge-transfer complex (**i**) in the solid state.

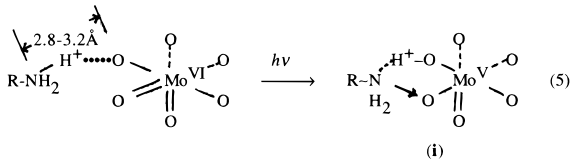

(**i**)

Complex (**i**) reflects the separation of the electron and hole charges which are produced by the O→Mo LMCT transition in the polyoxomolybdate lattice. It is this separation which keeps the colored state stable. The bleaching which occurs in the presence of oxygen molecules is caused by the back reaction which is triggered by an electron transfer from the Mo^V atom to the oxygen molecule. The irreversibility for $[NH_3Me]_8[Mo_8O_{26}(MoO_4)_2]\cdot 2H_2O$ (Table 2) suggests that the methylammonium cation undergoes photochemical oxidative decomposition. The bleaching mechanism of this compound remains unclear.

The observable ESR spectra of the UV-irradiated single crystals of alkylammonium polyoxomolybdates at room temperature are exemplified in Figure 5. The spectrum with $^{95,97}Mo$ and ^1H hyperfine structures at room temperature indicates that the single unpaired electron resides in an orbitally nondegenerate ground state for a single $MoO_5(OH)$ site in the anion. Each spectrum can be interpreted using the spin Hamiltonian in eq 6 with $S = {}^1/_2$, $I_{Mo} = {}^5/_2$, and $I_H = {}^1/_2$.

$$H = \beta H\cdot g\cdot S + I_{Mo}\cdot A_{Mo}\cdot S + \sum_H I_H\cdot A_H\cdot S \quad (6)$$

The final ESR parameters were obtained by an iterative least-squares procedure utilizing exact diagonalizations of the Hamiltonian matrix and are given in Table 3.

The structure of the paramagnetic site in the polyoxomolybdate anion was elucidated for the $Mo^VO_4(OH)_2$ center in a UV-irradiated single crystal of $[NH_3Pr^i]_6[Mo_8O_{26}(OH)_2]\cdot 2H_2O$.[89] The ESR spectrum of this crystal at room temperature indicates that two magnetically equivalent protons interact with a paramagnetic electron localized at the distorted $MoO_5(OH)$ octahedral site. One of the two protons was the original hydroxo proton, while the other is originally a hydrogen-bonding $[NH_3Pr^i]^+$ proton which transferred to a bridging oxygen atom trans to the hydroxo group. Analysis of the ESR parameters g, ^{95}Mo and ^{97}Mo hyperfine, and ^1H superhyperfine tensors using a point-dipole approxi-

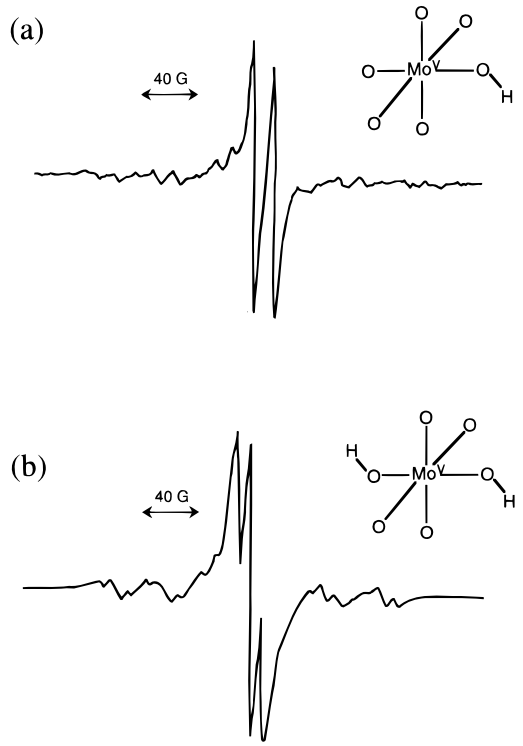

Figure 5. ESR spectra of UV-irradiated single crystals of $[NH_3Pr]_6[Mo_7O_{24}]\cdot 3H_2O$ (a) and $[NH_3Pr^i]_6[Mo_8O_{26}(OH)_2]\cdot 2H_2O$ (b) at room temperature. The signals indicate $g = 1.921$, $A_{Mo} = 42.2$ G, and $A_H = 14.1$ G (a) and $G = 1.940$, $A_{Mo} = 34.0$ G, and $A_H = 9.0$ G (b).

mation for the low-symmetric site indicates that the maximum eigenvector of the ^1H superhyperfine tensors with all positive signs lies close to the $Mo^V\cdots H^+$ direction and that the superhyperfine couplings with the proton nuclei arise from a direct participation of the H 1s orbital in the semioccupied molecular orbital. The eigenvectors of the intermediate component for the A_{Mo} tensors are close to the Mo···O molecular axis involving the oxygen atom bonded to the transfered proton, and the eigenvector of the lowest component for the A_H tensors is close to the Mo···O axis involving the oxygen atom which interacts with the amino nitrogen atom in the charge-transfer complex (**i**). The semioccupied molecular orbital (SOMO) of the paramagnetic electron consists primarily of the extensively mixed d orbitals (>90%), along with the oxygen and nitrogen 2p orbitals (a significant contribution), the Mo 5s orbital, and the H 1s orbital. The extended-Hückel calculations for the molybdenum(V) site indicate that the two protons at the paramagnetic site are situated symmetrically at a distance of about 1.9 Å from the paramagnetic molybdenum atom and 1.43 Å from the nearest oxygen atom. This is rather long for an O−H bond and results from the significant mixing of the Mo 4d and O and N 2p orbitals in the SOMO. The structural configuration of the paramagnetic site corresponds to the molecular structure at the saddle zone in the full potential energy surface, which can be regarded as a transition state for the photoredox reaction in solutions.[89] Figure 6 shows the environment of the $Mo^VO_5(OH)$ site in its photoinduced colored state, along with the approximate directions of selected eigenvectors for the A_H and A_{Mo} tensors,

Table 3. ESR Parameters for the Mo^V Centers in UV-Induced Alkylammonium Polyoxomolybdate Lattices[a]

principal values		$[NH_3Pr^i]_6[Mo_7O_{24}]\cdot 3H_2O$ site A	$[NH_3Pr^i]_6[Mo_7O_{24}]\cdot 3H_2O$ site B	$[NH_3Pr]_6[Mo_7O_{24}]\cdot 3H_2O$	$[NH_3Pr^i]_6[Mo_8O_{26}(OH)_2]\cdot 2H_2O$	$[NH_3Me]_8[Mo_8O_{26}(MoO_4)_2]\cdot 2H_2O$ site A	$[NH_3Me]_8[Mo_8O_{26}(MoO_4)_2]\cdot 2H_2O$ site B
g	g_1	1.899	1.898	1.895	1.901	1.899	1.899
	g_2	1.924	1.922	1.925	1.935	1.930	1.930
	g_3	1.935	1.936	1.937	1.958	1.949	1.949
	g_0	1.919	1.919	1.919	1.931	1.926	1.926
A_{Mo}	A_{Mo1}	30.7	28.5	23.4	19.4	23.7	28.0
	A_{Mo2}	34.0	37.1	42.0	35.9	40.2	41.8
	A_{Mo3}	74.5	74.7	69.9	76.8	73.5	76.8
	A_{Mo0}	46.4	45.8	45.1	44.0	45.8	48.9
A_H	A_{H1}	6.36	5.98	8.15	6.78	6.57	6.87
	A_{H2}	8.63	9.39	9.14	8.41	10.7	9.69
	A_{H3}	11.85	11.58	12.5	8.94	12.4	12.3
	A_{H0}	8.95	8.98	9.93	8.05	9.86	9.63

[a] $g_0 = (g_1 + g_2 + g_3)/3$; units of A are 10^{-4} cm^{-1}, $A_{Mo0} = (A_{Mo1} + A_{Mo2} + A_{Mo3})/3$ and $A_{H0} = (A_{H1} + A_{H2} + A_{H3})/3$.

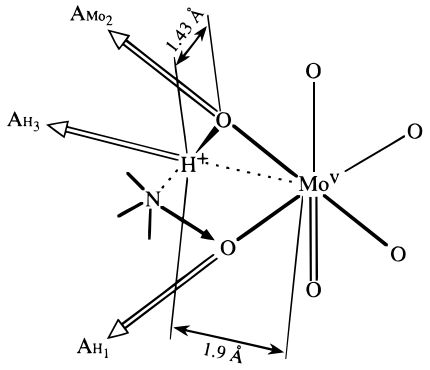

Complex (**i**)

Figure 6. Schematic environment of the UV-induced $Mo^VO_5(OH)$ site and approximate directions of the selected eigenvectors of ESR parameters. A_{H1} and A_{H3} indicate the minimum and maximum eigenvectors of ^1H superhyperfine tensors, and A_{Mo2} indicates the intermediate component for the A_{Mo} tensors.

as determined for the photoreducible MoO_6 site in a variety of alkylammonium polyoxomolybdate lattices.

The relative rate of coloration for the alkylammonium polyoxomolybdates correlates with the number of the photoreducible MoO_6 sites in the respective edge-shared MoO_6 octahedral polyoxomolybdate anions. Table 2 shows the agreement between the relative rates of UV-induced coloration for $[NH_3Pr^i]_6[Mo_7O_{24}]\cdot 3H_2O$, $[NH_3Pr]_6[Mo_7O_{24}]\cdot 3H_2O$, $[NH_3Pr^i]_6[Mo_8O_{26}(OH)_2]\cdot 2H_2O$, and $[NH_3Me]_8[Mo_8O_{26}(MoO_4)_2]\cdot 2H_2O$ and the number of the photoreducible MoO_6 sites in the anion (1, 1, 2, and 4, respectively, as marked by an asterisk (*) in Figure 4). The number of sites were determined by analysis of the ESR spectra of UV-irradiated single crystals of the compounds. The ammonium salts of polyoxomolybdates are not UV sensitive; however, under γ-ray irradiation, they yield paramagnetic sites similar to those discussed above, as has been shown for $[NH_4]_6[Mo_7O_{24}]\cdot 4H_2O$.[90,91] The lack of UV sensitivity exhibited by the NH_4^+ polyoxomolybdate salts can be attributed to the chemical instability of the charge-transfer complex (**i**), which results in the preferential recombination of the d^1 electron and the 2p hole at the MoO_6 site. ENDOR results for the γ-irradiated single crystal of $[NH_4]_6[Mo_7O_{24}]\cdot 4H_2O$ indicate that a $MoO_5(OH)$ center is formed at one of the four MoO_6 octahedra having C_4 symmetry within the C_{2v} symmetry anion. This center is formed as a result of direct decomposition of an NH_4^+ ion.[92] The proton is estimated to be 1.46 Å from the terminal O atom, which is close to the limits of applicability of the point−dipole approximation. The γ-induced paramagnetic site in the Mo_7O_{24} framework of the $[NH_4]_6[Mo_7O_{24}]\cdot 4H_2O$ solid occupies a location different from that of the UV-irradiated $[NH_3Pr]_6[Mo_7O_{24}]\cdot 3H_2O$ solid. The UV-induced paramagnetic site lies at the end of three MoO_6 octahedra which form a line at the central horizontal level (Figure 4). These differences in the location of the paramagnetic site are the result of differences in the hydrogen-bonding network between the NH_4^+ and alkylammonium salts in the lattice. None of tetrabutylammonium salts of polyoxomolybdates exhibit UV-induced coloration in the solid state. Thus, the presence of a transferable proton in a hydrogen bond between the polyoxometalate anion and alkylammonium cation is essential to keeping the d^1 electron localized at the MoO_6 octahedron and allowing UV-induced coloration to occur. The $[NHEt_3]_3[H_3O][Mo_8O_{26}]\cdot 2H_2O$ solid,[93] which was a H_3O cation connecting the two independent β-$[Mo_8O_{26}]^{4-}$ anions via complicated hydrogen bonds, is also photosensitive and turns from white to brown.

The colors of the UV-irradiated polyoxomolybdate solids are related to the extent of delocalization of the d^1 electron, which is governed by the M−O−M bond angle and reflects the $d\pi-p\pi-d\pi$ orbital mixing in the polyoxometalates.[94−98] In the edge-shared MO_6 octahedral lattices with M−O−M bond angles of about 100°, the d^1 electron is localized at almost a single MO_6 octahedron site, which results in the reddish brown color seen for $[NH_3Pr^i]_6[Mo_8O_{26}(OH)_2]\cdot 2H_2O$.[89] On the other hand, the Keggin framework, involving a corner-shared linkage of different M_3O_{13} groups, allows thermally activated, electron-hopping delocalization between corner-shared MO_6 octahedra with M−O−M bond angles of 150°. This results in a blue UV-induced coloration as observed for $[NH_3Pr^i]_3[PMo_{12}O_{40}]$ and $[NH_3Pr^i]_4[SiMo_{12}O_{40}]$. Similar behavior is observed in the lattices containing the Keggin structural anion and organic molecules,

such as $H_3[Mo_{12}O_{40}]\cdot 6$(tetramethylthiourea),[99] $H_3[PMo_{12}O_{40}]\cdot 6DMA\cdot CH_3CN\cdot 0.5H_2O$ (DMA = *N*,*N*-dimethylacetamide),[100] and $[(DP)_2H]_3[PW_{12}O_{40}]$ (DP = dipolar organic media such as *N*-methylpyrrolidinone, 1,1,3,3-tetramethylthiourea, and 1,3-dimethyl-2-imidazolidinone).[101]

B. Other Polyoxometalates

A UV-induced color change from white to brown is observed for a variety of anilinium and pyridinium salts of β-octamolybdates $[NH_3C_6H_5]_4[Mo_8O_{26}]\cdot 2H_2O$,[102] $[NHMe_2C_6H_5]_4[Mo_8O_{26}]\cdot 2H_2O$,[103] $[NHC_5H_4(3\text{-}Me)]_4[Mo_8O_{26}]$,[104] $[NHC_5H_4(4\text{-}Me)]_4[Mo_8O_{26}]$,[105] $[NHC_5H_4(3\text{-}Me)]_x[NHC_5H_4(3\text{-}Et)]_{4-x}[Mo_8O_{26}]$ (x = 0, 2, 3, 4),[106] and $[NHC_5H_4(3\text{-}NH_2)]_4[Mo_8O_{26}]\cdot 2DMF$ (DMF = *N*,*N*-dimethylformamide).[107] This coloration can be attributed to a transfer of the proton involved in the hydrogen bond between the anion and the organic cation, as was described for the alkylammonium salts of polyoxomolybdates. Similarly, alkylammonium salts of polyoxovanadate and -tungstate lattices undergo UV-induced coloration, such that $[NH_3Bu^t]_4[V_4O_{12}]$ turns from white to brown[108,109] and $[NHBu_3]_4[W_{10}O_{32}]$ turns from white to blue. UV-induced coloration also occurs in polyoxometalates which are coordinated to organic ligands: $[NH_4]_3[Mo_8O_{26}(HCO_2)_2]\cdot 2H_2O$ (white → reddish brown);[110] $Na_4[Mo_8O_{24}(OMe)_4]\cdot 8H_2O$ (white → blue);[111] $[Hpy]_4[Mo_8O_{26}(py)_2]\cdot 8Me_2SO$ (py = pyridine),[112] $[NH_3Pr]_2[H_4Mo_8O_{26}(OC_6H_4CH{=}NPr\text{-}2)_2]\cdot 6MeOH$ ($(OC_6H_4CH{=}NPr\text{-}2)$ = *N*-propylsalicylideneiminate),[113] $[Hmorph]_4[Mo_8O_{24}(MetO)_2]\cdot 4H_2O$ (morph = morpholine and MetO = methioninate),[113] $Na_2[Mo_8O_{26}(H_2Lys)_2]\cdot 8H_2O$ (Lys = lysine) (white → brown);[114] and $Na_2[(Hamp)_2Mo_5O_{15}]\cdot 6H_2O$ (amp = adenosine-5′-monophosphate) (white → blue).[115] Although other organic−inorganic charge-transfer salts based on polyoxometalates such as β-$[Htmpd]_x[tmpd]_{3-x}[HMo_8O_{26}]$ (tmpd = *N*,*N*,*N*′,*N*′-tetramethyl-*p*-phenylenediamine) have been prepared in an attempt to achieve perfectly reversible photochromism in the absence of oxygen molecules, this goal has not been realized and UV coloration remains largely irreversible.[116]

IV. Electrochromism of Polyoxometalates

A. $H_3PW_{12}O_{40}$

$H_3PW_{12}O_{40}$ is an electrochromic and ionic conductive material.[117] A typical cell for this material is fabricated by placing the $H_3PW_{12}O_{40}$ in a 3-mm bore ceramic tube and compressing it at ∼500 kg cm^{-2} against a transparent conducting SnO_2 electrode deposited on a glass slide (see Figure 7a). The SnO_2 layer constitutes the front, or viewing, electrode. Metallic Cu or Ag, or a nonstoichiometric mixed conductor capable of providing Li^+, Cu^+, and Ag^+ ions (such as $Li_xV_yCr_{1-y}S_2$, $Cu_{2-x}Se$, or $Ag_{2-x}Se$), is then applied as the back or counter electrode. The cell characteristics are independent of the nature of the counter electrode. Typically, the $H_3PW_{12}O_{40}$ layer, which is in contact with the SnO_2 electrode, changes color when the SnO_2 is biased to −1 V with respect to the Ag electrode. Likewise, it bleaches when the SnO_2 is biased to +2.5 V. A coloration charge of ∼1 mC/cm^2 was measured at a ∼0.3 reduction in diffuse reflectivity at 1000 nm. This allows the minimum thickness of the colored layer to be estimated at ∼500 Å. Thus, the area density of color centers is ∼10^{16} cm^{-2}, which is comparable to the composition of $M_{\sim 0.1}WO_3$ in 3000 Å thick films which is required for adequate contrast in WO_3-based cells. The $H_3PW_{12}O_{40}$-based cells show useful response times of 50 ms. However, these cells have a disadvantage in that they bleach relatively slowly when heavily colored.

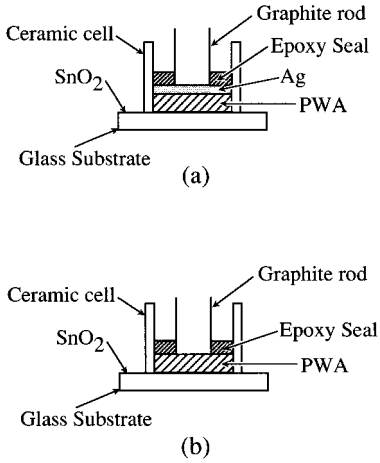

Figure 7. A schematic configuration of the electrochromic cell based on $H_3PW_{12}O_{40}$.

Both solid-state and simplified cells have been fabricated in an attempt to improve the electrochromic properties of $H_3PW_{12}O_{40}\cdot 29H_2O$ and $H_3PMo_{12}O_{40}\cdot 29H_2O$ systems.[118] In the cell diagrammed in Figure 7b, the back electrode is graphite powder or simply a graphite rod, and the entire cell is sealed with epoxy resin. A bleaching voltage of ∼1.2 V was applied to this cell, while a coloring pulse of >−2 V was applied for 0.1 s at a repetition rate of 0.5−1 Hz. A −1.2 V coloring voltage with an average current of 10 mA produced a ∼50% decrease in reflectivity at 800 nm in 10 ms. The integrated charge was ∼1 mC/cm^2 for a cell area of 0.1 cm^{-2}. These values compare favorably with the WO_3 liquid electrolyte cells. Oxidation occurs at the carbon electrode to maintain charge neutrality in the cell as a whole, during coloration. Since there are hydroxy groups on the carbon surface, a liberated proton can be injected into the $H_3PW_{12}O_{40}$ layer, with the electron completing the external circuit. The net electrochemical reaction is

$$C{-}OH + H_3PW_{12}O_{40} \rightleftharpoons C{=}O + H_4PW_{12}O_{40} \quad (7)$$

The critical feature in these cells is the contact between $H_3PW_{12}O_{40}$ and SnO_2. The cell's shelf life is limited by an increase in cell impedance over time.

B. $K_{0.33}WO_{3.165}$ and Peroxopolytungstic Acids

$K_{0.33}WO_{3.165}$ is an electrochromic material which is prepared by cathodically depositing a reduced decatungstate $K_4[HW_{10}O_{32}]/K_5[HW_{10}O_{32}]$ film on an ITO electrode and then heating it at 400 °C in air.[119]

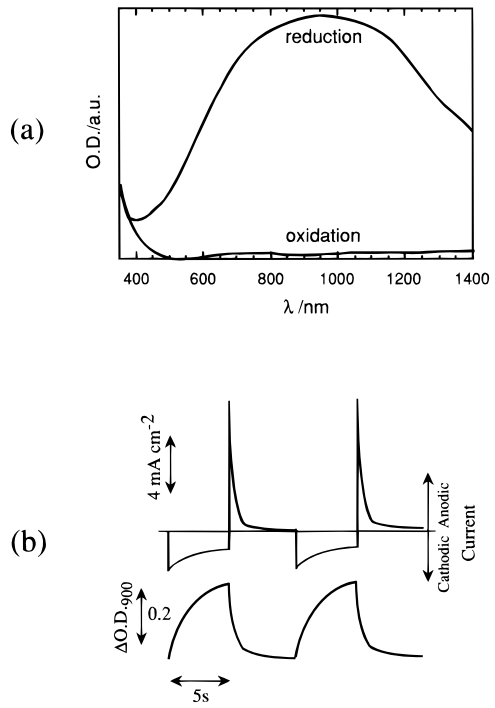

Figure 8. Absorption spectral change (a) of the evaporated $K_{0.33}WO_{3.165}$ film ($d = 2\ \mu$m) electrode and its current and absorbance (at 900 nm) time transients (b) at $U_{Ag} = -0.6$ V (5 s) and 1.2 V (5 s) repetitive potential steps.

$K_{0.33}WO_{3.165}$ also can be prepared by the thermal reaction of WO_3 and K_2CO_3 in the ratio of 6:1 at a much higher temperature (800 °C).[120] The coloration reaction is denoted by eq 8.

$$K_{0.33}WO_{3.165}\ (\text{bleached}) + H_2O + e^- \rightarrow K_{0.33}HWO_{3.165}\ (\text{dark blue}) + OH^- \quad (8)$$

The H_2O molecule exists as a contaminate in the crystal lattice or propylene carbonate electrolyte and donates an H^+ during the reductive coloration of $K_{0.33}WO_{3.165}$. $K_{0.33}WO_{3.165}$ films grown by evaporating $K_{0.33}WO_{3.165}$ powder in a vacuum, followed by annealing at 150 °C for 4 h, provide an optimum water content in the film. Figure 8 shows the absorption spectra of such a film at $U_{Ag} = -0.6$ V (reduction) and +1.2 V (oxidation) in an electrochemical cell containing 1 M $LiClO_4$ in propylene carbonate. The electrochromism of $K_{0.33}WO_{3.165}$ is comparable to that of the amorphous WO_3 liquid electrolyte system.[121]

Spin-coating a solution of tungsten or tungsten carbide powder in a 15% H_2O_2 is the best method for fabricating large-scale electrochromic devices.[122] The homogeneous thin films formed in this manner consist of amorphous peroxopolytungstic acids, and their electrochromic properties are similar to those of amorphous WO_3 films.[123]

V. Photoluminescence and Intramolecular Energy Transfer in Polyoxometalate Solids

A. Polyoxometalloeuropates

When several energy levels exist within the O→M LMCT bands in the polyoxometalate lattices, energy transfer from the O→M LMCT excited states to these levels may be possible (Figure 1). In fact, this process is observed during the sensitized luminescence of Eu^{3+},[123−138] Mn^{4+},[139] and Cr^{3+} [140,141] as a result of intramolecular energy transfer within their respective polyoxometallometalates.

Early studies of the intramolecular energy-transfer processes in decatungstolanthanoates $[[LnW_{10}O_{36}]^{9-}$ $(=[Ln(W_5O_{18})_2]^{9-})]$, indicated that the Eu^{3+} complex $[EuW_{10}O_{36}]^{9-}$ was the most luminescent of the $[LnW_{10}O_{36}]^{9-}$ anions when the O→W LMCT bands were photoexcited.[124−129,142,143] The Gd^{3+} complex $[GdW_{10}O_{32}]^{9-}$ exhibited tungstate emission instead of Gd^{3+} emission.[125,126] Low yields were obtained for the sensitized emission of Ln^{3+} from the other decatungstolanthanoates due to radiationless loss via charge-transfer states Ln^{4+}−W^{5+} in the Pr^{3+} and Tb^{3+} complexes and cross relaxation in the Sm^{3+}, Dy^{3+}, and Ho^{3+} complexes.[125] The luminescence spectrum of $[EuW_{10}O_{36}]^{9-}$ was analyzed with the help of the crystal structure of $Na_6H_2[CeW_{10}O_{36}]\cdot 30H_2O$.[144] Sensitized luminescence of Eu^{3+} was also observed for the $[Eu(SiW_{11}O_{39})_2]^{13-}$, $[Eu(BW_{11}O_{39})_2]^{15-}$, and $[Eu(P_2W_{17}O_{61})_2]^{17-}$ anions, which contain an Eu^{3+} ion surrounded by two lacunary polyoxometalates, $[SiW_{11}O_{39}]^{8-}$, $[BW_{11}O_{39}]^{9-}$, and $[P_2W_{17}O_{61}]^{10-}$, respectively.[124−128] It is expected that the Eu-encrypted Preyssler complex $[EuP_5W_{30}O_{110}]^{12-}$, which consists of a cyclic arrangement of five PW_6O_{22} units each with D_{5h} symmetry, will also exhibit sensitized luminescence since the lifetimes of the Eu^{3+} emission observed during direct excitation of Eu^{3+} ions in aqueous solutions of the complex imply the coordination of two or three aqua ligands per Eu^{3+}.[145−147]

1. Structural Feature

The intramolecular energy transfer in polyoxometalloeuropate lattices has been systematically studied using six polyoxometalloeuropates: $Na_9[EuW_{10}O_{36}]\cdot 32H_2O$,[130] $K_{15}H_3[Eu_3(H_2O)_3(SbW_9O_{33})(W_5O_{18})_3]\cdot 25.5H_2O$,[131] $[NH_4]_{12}H_2[Eu_4(H_2O)_{16}(MoO_4)(Mo_7O_{24})_4]\cdot 13H_2O$,[136] $Eu_2(H_2O)_{12}[Mo_8O_{27}]\cdot 6H_2O$,[132] $Na_7H_{19}\{[Eu_3O(OH)_3(H_2O)_3]_2Al_2(Nb_6O_{19})_5\}\cdot 47H_2O$,[138] and $[Eu(H_2O)_8]_3K_2H_3[(GeTi_3W_9O_{37})_2O_3]\cdot 13H_2O$.[139] Figure 9 shows the six anions as assemblies of linked MO_6 octahedra, along with the coordination shape of the Eu atom in the anion. In $Na_9[EuW_{10}O_{36}]\cdot 32H_2O$, four O atoms from the W_5O_{18} group of the half anion are bonded to the Eu atom, resulting in 8-fold coordination of Eu^{3+}. There is no water molecule in in the first coordination sphere of the Eu^{3+}, and the anion has an approximate point symmetry of C_{4v}.[130] In the anion of $K_{15}H_3[Eu_3(H_2O)_3(SbW_9O_{33})(W_5O_{18})_3]\cdot 25.5H_2O$, a central trinuclear $Eu_3(H_2O)_3$ core is tetrahedrally linked to three W_5O_{18} groups and one B-α-type SbW_9O_{33} group, giving it an approximate point symmetry of C_{3v}.[131] The SbW_9O_{33} group is a trivacant B-α-type ligand which contains a tricoordinated Sb^{3+} ion and three corner-sharing W_3O_{13} groups, each comprised of three edge-shared WO_6 octahedra. Each Eu^{3+} in the $Eu_3(H_2O)_3$ core achieves 8-fold coordination by attachment to four oxygens from one W_5O_{18}, two oxygens from one SbW_9O_{33}, and two aqua oxygens ligands. In $[NH_4]_{12}H_2[Eu_4(H_2O)_{16}(MoO_4)(Mo_7O_{24})_4]\cdot 13H_2O$ the anion con-

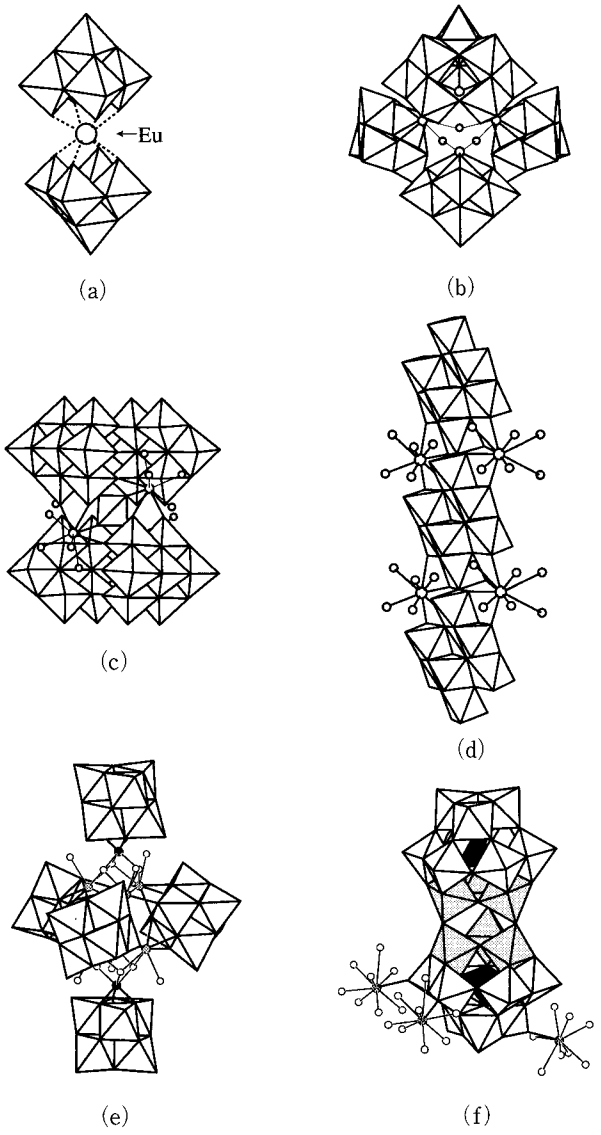

Figure 9. Structures of anions for six polyoxometalloeuropate complexes: $[EuW_{10}O_{36}]^{9-}$ (a), $[Eu_3(H_2O)_3(SbW_9O_{33})(W_5O_{18})_3]^{18-}$ (b), $[Eu_4(H_2O)_{16}(MoO_4)(Mo_7O_{24})_4]^{14-}$ (c), $Eu_2(H_2O)_{12}[Mo_8O_{27}]$ (d), $[\{Eu_3O(OH)_3(H_2O)_3\}_2Al_2(Nb_6O_{19})_5]^{26-}$ (e), and $[\{Eu(H_2O)_8\}_3[Ge_2Ti_6W_{18}O_{77}]]^{5-}$ (f). Shaded octahedra in f represent TiO_6 sites.

sists of a central $[Eu_4(MoO_4)(H_2O)_{16}]^{10+}$ unit and four Mo_7O_{24} groups and has an overall point symmetry of D_{2d}.[136] Each Eu^{3+} achieves 9-fold coordination by attachment to one oxygen atom from the MoO_4 tetrahedron, two oxygen atoms from a single Mo_7O_{24} group, two oxygen atoms from other Mo_7O_{24} groups, and four oxygen atoms from aqua ligands. The anion of $Eu_2(H_2O)_{12}[Mo_8O_{27}]\cdot 6H_2O$ is isostructural to that of $[NH_4]_6[Mo_8O_{27}]\cdot 4H_2O$.[85] Eu^{3+} is coordinated by six aqua oxygen atoms, two oxygen atoms of a Mo_8O_{27} unit, and one oxygen atom belonging to the MoO_6 octahedron of a neighboring Mo_8O_{27} unit. This results in the formation of an infinite belt of octamolybdate $\{[Mo_8O_{27}]^{6-}\}_\infty$ by the Eu^{3+}.[132] The anion of $Na_7H_{19}\{[Eu_3O(OH)_3(H_2O)_3]_2Al_2(Nb_6O_{19})_5\}\cdot 47H_2O$ consists of two $[Eu_3O(OH)_3(H_2O)_3]^{4+}$ clusters, two Al^{3+} cations, and five $[Nb_6O_{19}]^{8-}$ anions.[137] Each Eu^{3+} achieves 8-fold oxygen atom coordination via one μ_3-O ion, two OH^- ions, one terminal H_2O, and four oxygen atoms belonging to the equatorial $[Nb_6O_{19}]^{8-}$ groups.

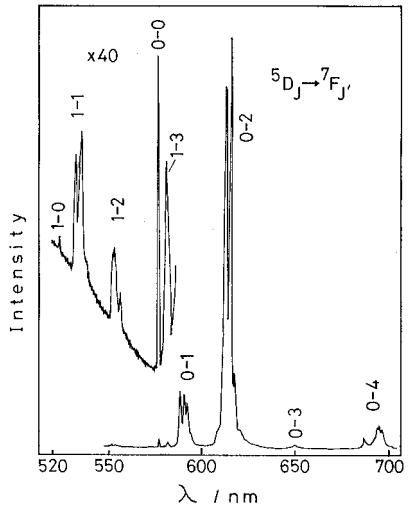

Figure 10. Luminescence spectrum of $Eu_2(H_2O)_{12}[Mo_8O_{27}]\cdot 6H_2O$ at 77 K under the O→Mo LMCT band excitation.

The anion of $[Eu(H_2O)_8]_3K_2H_3[(GeTi_3W_9O_{37})_2O_3]\cdot 13H_2O$[138] is a condensed aggregate of Keggin-type $[GeTi_3W_9O_{37}]^{9-}$ ions,[148] and the Eu^{3+} is coordinated to a terminal oxygen atom of $[(GeTi_3W_9O_{37})_2O_3]^{14-}$ and eight aqua oxygen atoms. As shown in Figure 9, the local symmetry around the Eu^{3+} in $Na_9[EuW_{10}O_{36}]\cdot 32H_2O$ and $K_{15}H_3[Eu_3(H_2O)_3(SbW_9O_{33})(W_5O_{18})_3]\cdot 25.5H_2O$ is approximately square antiprismatic, while it is approximately tricapped trigonal-prismatic in $[NH_4]_{12}H_2[Eu_4(H_2O)_{16}(MoO_4)(Mo_7O_{24})_4]\cdot 13H_2O$, $Eu_2(H_2O)_{12}[Mo_8O_{27}]\cdot 6H_2O$, and $[Eu(H_2O)_8]_3K_2H_3[(GeTi_3W_9O_{37})_2O_3]\cdot 13H_2O$ and approximately bicapped trigonal-prismatic in $Na_7H_{19}\{[Eu_3O(OH)_3(H_2O)_3]_2Al_2(Nb_6O_{19})_5\}\cdot 47H_2O$.

2. Intramolecular Energy Transfer from the O→M LMCT States to Eu^{3+}

Photoexcitation of the O→M (M = Nb, Mo, W) LMCT bands of the polyoxometalloeuropates leads to an Eu^{3+} emission with a single exponential decay.[131−135] The emission originates from both the $^5D_0$ and $^5D_1$ excited states of Eu^{3+}, and the luminescent transitions all terminate in the $J = 0-4$ levels of the ^7F_J ground state. Figure 10 shows the photoluminescence spectrum of $Eu_2(H_2O)_{12}[Mo_8O_{27}]\cdot 6H_2O$ at 77 K. $Na_9[EuW_{10}O_{36}]\cdot 32H_2O$, which has an anhydrous Eu^{3+} site, exhibits the high quantum yield (≈1.0 at 4.2 K) for the emission corresponding to the O→W LMCT band excitation, and the intensity of the $^5D_0 \rightarrow ^7F_1$ emission is the highest among the $^5D_0 \rightarrow ^7F_J$ transitions.[124−130] The intensity of the $^5D_0 \rightarrow ^7F_1$ transition depends only slightly on the nature of the surroundings of the Eu^{3+}, since the $^5D_0 \rightarrow ^7F_1$ transition is of almost magnetic dipole character.[149,150] By using the intensity of the $^5D_0 \rightarrow ^7F_1$ magnetic dipole transition for $Na_9[EuW_{10}O_{36}]\cdot 32H_2O$ as a standard, the radiative (k_{rad}) and nonradiative (k_{nr}) rates for the $^5D_0$ state and the quantum yield (Φ_{et}) of the overall energy transfer from the O→M LMCT states to the $^5D_0$ state (in part through the $^5D_1$ state) can be calculated from the relative intensities of the $^5D_0 \rightarrow ^7F_J$ transitions, the quantum yields, and the lifetimes of the $^5D_0 \rightarrow ^7F_J$ emission.[151] Table 4 displays the calculated values of k_{rad}, k_{nr}, and Φ_{et} as well as

Table 4. Radiative Rate (k_{rad} in s^{-1}), Nonradiative Rate (k_{nr} in s^{-1}), and Ratio (η_{rad}) of Radiation of the $^5D_0$ State of Eu^{3+} and Quantum Yield (Φ_{et}) of the Overall Energy Transfer from O→M LMCT States to the $^5D_0$ State (through the $^5D_1$ state in part) for 1−6[a,b]

	1	2	3	4	5	6
n	0	2	4	6	1, (2)[b]	8
τ						
4.2 K	3.7	1.1 ± 0.2		0.16	0.32 ± 0.01	0.15 ± 0.01
77 K	3.3	1.1 ± 0.2	0.24 ± 0.02	0.17 ± 0.01	0.31 ± 0.01	0.14 ± 0.01
300 K	2.8	1.1 ± 0.2	0.20 ± 0.01	0.17 ± 0.01	0.31 ± 0.02	0.14 ± 0.01
k_{rad}	2.7×10^2	7.5×10^2	1.1×10^3	9.0×10^2	1.4×10^3	7.9×10^2
k_{nr}						
4.2 K	≈0	$(1.9 \pm 1.7) \times 10^2$		5.4×10^3	$(1.7 \pm 0.1) \times 10^3$	$(5.9 \pm 0.4) \times 10^3$
77 K	3×10	$(1.9 \pm 1.7) \times 10^2$	$(3.2 \pm 0.3) \times 10^3$	$(5.0 \pm 0.3) \times 10^3$	$(1.8 \pm 0.1) \times 10^3$	$(6.4 \pm 0.5) \times 10^3$
300 K	9×10	$(1.9 \pm 1.7) \times 10^2$	$(4.0 \pm 0.2) \times 10^3$	$(5.0 \pm 0.3) \times 10^3$	$(1.8 \pm 0.2) \times 10^3$	$(6.4 \pm 0.5) \times 10^3$
η_{rad}						
4.2 K	1.0	0.83 ± 0.15		0.14 ± 0.01	0.45 ± 0.01	0.12 ± 0.01
77 K	0.90	0.83 ± 0.15	0.25 ± 0.02	0.15 ± 0.01	0.43 ± 0.01	0.11 ± 0.01
300 K	0.75	0.83 ± 0.15	0.21 ± 0.01	0.15 ± 0.01	0.44 ± 0.03	0.11 ± 0.01
Φ_{et}						
4.2 K	1.0	0.69 ± 0.12		0.24 ± 0.01	0.19 ± 0.01	$(6 \pm 1) \times 10^{-3}$
77 K	1.0	0.64 ± 0.12	0.48 ± 0.04	0.19 ± 0.01	0.09 ± 0.01	$(2 \pm 1) \times 10^{-3}$
300 K	0.94	0.31 ± 0.06	0.33 ± 0.02	0.08 ± 0.01	0.02	

[a] Since the relative intensities of $^5D_0 \rightarrow {}^7F_J$ emission was hardly changed on a variety of temperature, k_{rad} was evaluated to be independent on the temperature. [b] Number of hydroxo ligands: $Na_9[Eu(W_5O_{18})_2]\cdot 32H_2O$ (**1**), $K_{15}H_3[Eu_3(H_2O)_3(SbW_9O_{33})(W_5O_{18})_3]\cdot 15.5H_2O$ (**2**), $(NH_4)_{12}H_2[Eu_4(H_2O)_{16}(MoO_4)(Mo_7O_{24})_4]\cdot 13H_2O$ (**3**), $Eu_2(H_2O)_{12}[Mo_8O_{27}]\cdot 6H_2O$ (**4**), $Na_7H_{19}[\{Eu_3O(OH)_3(H_2O)_3\}_2Al_2(Nb_6O_{19})_5]\cdot 47H_2O$ (**5**), and $K_2Eu_3H_3[Ge_2Ti_6W_{18}O_{77}]\cdot 37H_2O$ (**6**).

the number (n) of aqua and hydroxo ligands bound to Eu^{3+}, and the lifetimes (τ in unit of ms) at 4.2, 77, and 300 K of the six polyoxometalloeuropate compounds.

The increase in the value of k_{nr} with increasing n value is due to the radiationless deactivation of the $^5D_0$ state through weak vibronic coupling with the vibrational states of the aqua and hydroxo ligands' high-frequency OH oscillators. The $^5D_0-{}^7F_0$ energy difference is approximately equal to five times the highest vibrational frequency of the surroundings.[132] This nonradiative process usually is called multiphonon emission. A plot of the deviation ($\Delta\tau^{-1}$) of the reciprocal $^5D_0$ lifetimes from that of standard, $Na_9[EuW_{10}O_{36}]\cdot 32H_2O$, versus the total number of aqua and hydroxo ligands coordinated to Eu^{3+} indicates a good linearity ($n = 1.05\Delta\tau^{-1}$) irrespective of the coordination geometry, as long as the mean distance between the Eu and the aqua or hydroxo oxygen atoms is less than 2.5 Å. This implies that the $\Delta\tau^{-1}$ value can be used to predict the number of aqua and hydroxo ligands coordinated to Eu^{3+}, regardless of the coordination geometry, for polyoxometaloeuropates not amenable to study by single-crystal X-ray methods.[151,152]

The observation of d^1 hopping delocalization in the polyoxometalate ligand indicates that Φ_{et} decreases with increasing temperature. Thermal deactivation of the O→M LMCT states by d^1 hopping occurs because of the small disparity between the excited and ground state electron configurations, which is reflected in the bond angle of the M−O−M or Eu−O−M linkage. Photoexcitation into the O→M LMCT bands allows the d^1 electron to hop to the Eu^{3+} site via the Eu−O−M linkage, if the Eu−O−M bond angles are about 150°. This is because $f\pi-p\pi-d\pi$ orbital mixing in the Eu−O−M linkage can occur in a manner similar to the $d\pi-p\pi-d\pi$ mixing which occurs at the corner-shared MO_6 octahedra when the M−O−M bond angles are about 150°. Consequently, the polyoxometaloeuropates with Eu−O−M bond angles of about 150° ($K_{15}H_3[Eu_3(H_2O)_3(SbW_9O_{33})(W_5O_{18})_3]\cdot 25.5H_2O$, $[NH_4]_{12}H_2[Eu_4(H_2O)_{16}(MoO_4)(Mo_7O_{24})_4]\cdot 13H_2O$, and $Eu_2(H_2O)_{12}[Mo_8O_{27}]\cdot 6H_2O$ exhibit a strong Φ_{et} temperature dependence.[132,134,135] Polyoxometalate ligands having only edge-shared MO_6 octahedra with M−O−M bond angles of about 100° show only a small Φ_{et} temperature dependence. This is due to localization of the d^1 electron at the MO_6 octahedron and can be seen for $Na_9[EuW_{10}O_{36}]\cdot 32H_2O$. The highly symmetrical polyoxometalate ligands favor the effective nonradiative deactivation of the O→M LMCT excitation energy due to a small disparity between the O→M LMCT excited and ground states. This results in low values of Φ_{et} with a strong temperature dependence and can be seen for $Na_7H_{19}\{[Eu_3O(OH)_3(H_2O)_3]_2Al_2(Nb_6O_{19})_5\}\cdot 47H_2O$ and $[Eu(H_2O)_8]_3K_2H_3[(GeTi_3W_9O_{37})_2O_3]\cdot 13H_2O$.[140,151]

B. O→M LMCT Triplet Emission

The first O→M LMCT emission observed was with $Na_9[GdW_{10}O_{36}]\cdot 18H_2O$.[125,126] Luminescence from the O→M LMCT states is observed with other polyoxometalates, especially at low temperatures, and $K_{5.5}H_{1.5}[SbW_6O_{24}]\cdot 6H_2O$, in particular, is highly photoluminescent.[140,153] Decays of the O→M LMCT emission can be described as the sum of two exponentials, unlike the Eu^{3+} luminescence of polyoxometalloeuropates which occurs as a single exponential decay. Table 5 shows the decay (τ_{CT}) and quantum yield (Φ_{CT}) of the O→M LMCT emission for a variety of polyoxometalates. The long decay times (several hundred microseconds) of the O→M LMCT emission originate from the triplet states. Similar decay times are observed for the nonmolecular WO_6 octahedral compounds, $Ba_2CaTe_{1-x}W_xO_6$, where O→W LMCT photoexcitation of the $^1A_{1g} \rightarrow {}^1T_{1u}$ transition results in a characteristic WO_6 blue-green emission from two $^3T_{1u}$ levels, each of which has a different exponential decay of 10−70 μs below 100 K.[154,155] The O→M

Table 5. Photoluminescence Maxima, Emission Decay (τ_{CT}), and Quantum Yield (Φ_{CT}) under the Excitation of the O→M LMCT Band for Nine Compounds[140]

compounds	emission (λ_{max}/nm)	$\tau_{CT}/\mu s$		ϕ_{CT}	
		4.2 K	77 K	4.2 K	77 K
$K_{5.5}H_{1.5}[SbW_6O_{24}]\cdot 6H_2O$	520	176 + 245	143 + 160	0.61	0.43
$Na_5[IMo_6O_{24}]\cdot 3H_2O$	670	133 + 246	110 + 189	2.6×10^{-2}	1.5×10^{-2}
$Na_3H_6[CrMo_6O_{24}]\cdot 8H_2O$	703.0, 704.2	143	87	5×10^{-3}	1×10^{-3}
$K_6[Mo_7O_{24}]\cdot 4H_2O$	700	169 + 209	142 + 190	9.4×10^{-2}	3.1×10^{-2}
$Cs_4[W_{10}O_{32}]\cdot nH_2O$ (n = 4 or 5)	660	203 + 306	157 + 217	6.4×10^{-2}	4.5×10^{-2}
$K_5[BW_{12}O_{40}]\cdot 15H_2O$	520	134 + 185	105 + 140	4×10^{-2}	2×10^{-4}
$K_3[PMo_{12}O_{40}]\cdot nH_2O$	510	64 + 190	43 + 87	2×10^{-2}	1×10^{-4}
$[NBu_4]_2[W_6O_{19}]$	520	102 + 158	45 + 146	7×10^{-4}	1×10^{-4}
$[NBu_4]_2[Mo_6O_{19}]$	530	107 + 250	88 + 159	1×10^{-4}	
$K_9H_5[(GeTi_3W_9O_{37})_2O_3]\cdot 16H_2O$[151]	570	91 + 140	10 + 30	5×10^{-3}	1×10^{-3}

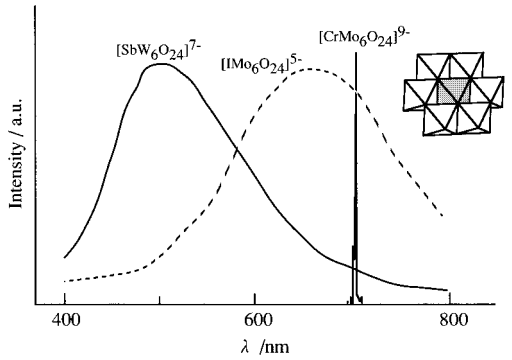

Figure 11. Photoluminescence spectra of $K_{5.5}H_{1.5}[SbW_6O_{24}]\cdot 6H_2O$, $Na_5[IMo_6O_234]\cdot 3H_2O$, and $Na_3H_6[CrMo_6O_{24}]\cdot 8H_2O$ solids at 4.2 K under 248 nm light irradiation. Polyhedral representation indicates Anderson-type structure $[XM_6O_{24}]^{n-}$ in which a central shaded octahedron is a heteroatom XO_6 site.

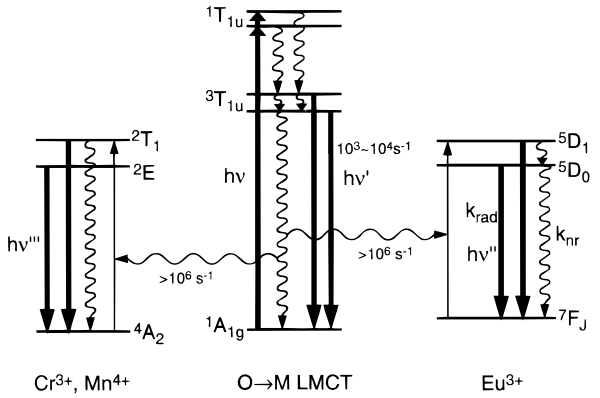

Figure 12. A schematic energy diagram of relaxation processes of the O→M LMCT excitation energy in a variety of polyoxometalate lattices.

LMCT triplet states of nonmolecular transition metal oxide have been identified with an empty d shell by ESR studies of the luminescent states of $K_2Cr_2O_7$, YVO_4, and $CaMoO_4$ crystals at 1.2 K.[156,162]

The involvement of the O→M LMCT triplet energy transfer in the polyoxometalate lattices was investigated using three isostructural Anderson-type complexes $K_{5.5}H_{1.5}[SbW_6O_{24}]\cdot 6H_2O$, $Na_5[IMo_6O_{24}]\cdot 3H_2O$, and $Na_3[H_6CrMo_6O_{24}]\cdot 8H_2O$.[114] Figure 11 shows the Anderson structure for the three compounds and their photoluminescence spectra under 248-nm light irradiation at 4.2 K. Photoexcitation of the O→M LMCT bands in the former two complexes lead to a broad emission due to the $^3T_{1u}\rightarrow{}^1A_{1g}$ transition which originates from the O→M LMCT triplet states. The green emission of $K_{5.5}H_{1.5}[SbW_6O_{24}]\cdot 6H_2O$ is intense and was observed even at room temperature, while $Na_5[IMo_6O_{24}]\cdot 3H_2O$ produced an orange emission only at low temperatures <100 K. The $Na_5[IMo_6O_{24}]\cdot 3H_2O$ emission produces small quantum yields compared to $K_{5.5}H_{1.5}[SbW_6O_{24}]\cdot 6H_2O$, and this is attributed to its small spin−orbit coupling and resultant increase in the nonradiative $^1T_{1u}\rightarrow{}^1A_{1g}$ transition probability. On the other hand, the $Na_3H_6[CrMo_6O_{24}]\cdot 8H_2O$ has a central Cr^{3+} which releases its transition energy within the O→Mo LMCT emission bands and does not show any O→Mo LMCT triplet emission. However, it does produce sharp $^2T_1$, $^2E\rightarrow{}^4A_2$ lines, known as R-lines, with single-exponential decays from the excited Cr^{3+} as a result of the energy transfer from the $^3T_{1u}$ O→Mo LMCT states. If the energy transfer from the O→Mo LMCT excited singlet state is operative in this case, one would expect the coexistence of both O→Mo LMCT triplet and Cr^{3+} luminescence, since the rate of the intersystem crossing for the $^1T_{1u}\rightarrow{}^3T_{1u}$ conversion would be high enough to compete with the energy transfer to Cr^{3+}. Therefore, the rate of the triplet energy transfer in $Na_3H_6[CrMo_6O_{24}]\cdot 8H_2O$ is estimated to be $>10^6$ s^{-1}. If it were not, the O→Mo LMCT triplet emission of $Na_3H_6[CrMo_6O_{24}]\cdot 8H_2O$ should be observed with nonexponential long decays of several hundred microseconds at <100 K.[140] The same is true for the polyoxometallomanganates such as $K_6Na_2[MnW_6O_{24}]\cdot 12H_2O$, $K_6[MnMo_6O_{32}]\cdot 6H_2O$, and $Na_{12}[Mn(Nb_6O_{19})_2]\cdot 50H_2O$, where the intramolecular energy transfer from the O→M (M = W, Mo, or Nb) LMCT triplet states into Mn^{4+} occurs to yield the R-line luminescence of Mn^{4+}.[139] Since the $^5D_0\rightarrow{}^7F_J$ transition energy of Eu^{3+} is close to the energy of the $^2T_1$, $^2E\rightarrow{}^4A_2$ transitions of Cr^{3+} and Mn^{4+}, it is reasonable to assume that the O→M LMCT triplet states are involved in the energy transfer in the polyoxometalloeuropate lattices. Figure 12 shows the energy transport processes for the O→M LMCT excitation in a variety of polyoxometalate lattices.[151]

VI. Photoinduced Formation of Heteropoly Blues

A. Polyoxomolybdates

UV irradiation of highly concentrated aqueous solutions of alkylammonium polyoxomolybdates results in the formation of blue species.[163−166] The deep, reddish-brown solids, which are obtained by UV

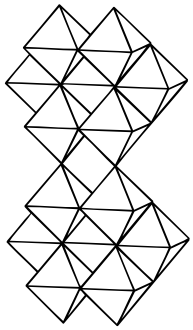

Figure 13. Polyhedral representation of the structure of $[Mo_{14}O_{46}]^{10-}$.

irradiation of alkylammonium polyoxomolybdate solids according to eq 5, form the same blue species on their dissolution in water.[78] ESR spin trapping reveals that photolysis of the solution results in the formation of an •OH radical accompanied by partial decomposition of the alkylammonium cation. Thus, it is proposed that the charge-transfer complex (**i**) in aqueous solution oxidizes the water to an •OH radical in competition with the deactivation to the original species and the decomposition of alkylammonium cation (eqs 9−11).

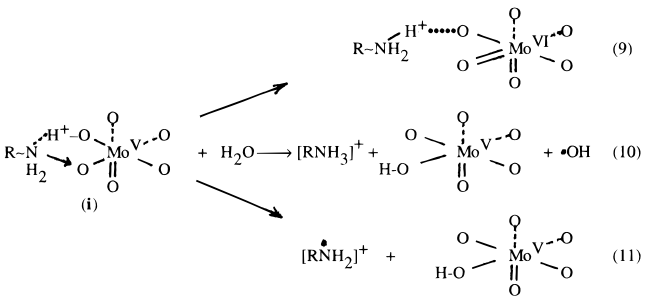

UV inactive $[NH_4]_6[Mo_7O_{24}]\cdot 4H_2O$ undergoes photoredox in the presence of electron-donating organic substances such as alcohols and carboxylic acids to yield $[Mo_7O_{23}(OH)]^{6-}$.[166−169] This one-electron-reduced $[Mo_7O_{23}(OH)]^{6-}$ anion is converted into a blue species. The blue species resulting from the photoredox reaction (eq 12) of $[NH_4]_6[Mo_7O_{24}]\cdot 4H_2O$ with MeOH has been characterized as the diamagnetic two-electron reduced species $[Mo_{14}O_{46}]^{10-}$.[170]

$$2[Mo_7O_{24}]^{6-} + MeOH \xrightarrow{h\nu} [Mo_{14}O_{46}]^{10-} + HCHO + 2OH^- \quad (12)$$

The structure of the anion of $[NMe_4]_2[NH_4]_8[Mo_{14}O_{46}]\cdot 8H_2O$ is shown in Figure 13. This $[Mo_{14}O_{46}]^{10-}$ (=$[(Mo_7O_{23})_2]^{10-}$) anion has a di-μ-oxobis(heptamolybdate) framework with an approximate symmetry of C_{2v}. The two electrons in the anion are located over the central two sets of MoO_6 octahedra, which are linked through an axial μ-oxo oxygen atom. The electronic structure returned by extended-Hückel calculations is in good agreement with the diamagnetic properties of this anion. Reduced anions consisting of four sets of two MoO_6 octahedra linked through an axial μ-oxo oxygen atom are found at the center of the nitrosyl decamolybdates $[Mo_{10}O_{25}(OMe)_6(NO)]^-$ and $[Mo_{10}O_{24}(OMe)_7(NO)]^{2-}$, which were prepared by the reduction of either $[Mo_5O_{13}(OMe)_4(NO)]^{2-}$ or $[Mo_6O_{18}(NO)]^{3-}$ with N_2H_4 in MeOH or $MeOH/CH_3CN$.[171] Other nitrosyl polyoxomolybdates, including $[Mo_{36}O_{108}(NO)_4(H_2O)_{16}]^{12-}$, $[Mo_{57}V_6O_{180}(NO)_6(OH)_3(H_2O)_{18}]^{21-}$, $[Mo_{57}Fe_6O_{174}(NO)_6(OH)_3(H_2O)_{24}]^{15-}$,[172] $\{[MoO_{2.5}(H_2O)][Mo_{36}O_{108}(NO)_4(H_2O)_{16}]^{12-}\}_\infty$,[173] and $[Mo_{154}O_{420}(NO)_{14}(OH)_{28}(H_2O)_{70}]^{(25\pm5)-}$ [174] have been prepared as novel, mesoscopic compounds by using $NH_2OH\cdot HCl$, $(N_2H_6)SO_4$, and $SnCl_2$ as the reducing agents.

An amorphous molybdenum blue is obtained upon photolysis of strongly acidic, aqueous molybdate solutions and may be related to $Na_{15}[Mo_{144}O_{409}(OH)_{28}(H_2O)_{56}]\cdot\sim 250H_2O$ which is reductively prepared using iron powder.[175] Other reduced polyoxometalates, such as the two-electron-reduced anions, α-$[H_2AsMo_{12}O_{40}]^{3-}$[176] and α-$[HPMo_{12}O_{40}]^{4-}$,[177] and the four-electron-reduced anions β-$[H_3PMo_{12}O_{40}]^{4-}$,[178] β-$[H_4AsMo_{12}O_{40}]^{3-}$,[176] and α-$[H_3S_2Mo_{18}O_{62}]^{5-}$ [177] have been prepared as disordered solids by electrolysis and chemical reduction methods.

B. Polyoxotungstates

The "polytungstate-Y" compound $[W_{10}O_{32}]^{4-}$ shows a strong O → W LMCT band (λ_{max} = 323 nm, ϵ = 1.35 × 10^4 dm^3 mol^{-1} cm^{-1} in CH_3CN) in the ultraviolet region and undergoes electrochemically quasi-reversible reduction with two successive steps (at −0.85 and −1.35 V vs Ag−AgCl in CH_3CN) in nonhydrolytic solvents. Each reduction yields a blue species.[179−182] The relatively low value of the O→W LMCT transition energy for $[W_{10}O_{32}]^{4-}$ makes it a good photocatalyst candidate for solar energy conversion. This is reinforced by the action spectrum of the anodic photocurrent observed for solutions containing $[W_{10}O_{32}]^{4-}$.[181−183] The oxidation potential of the one-electron-reduced species is highly negative compared to the redox potential of H^+/H_2, which indicates that $[W_{10}O_{32}]^{4-}$ is a simple photocatalyst for H_2 production from a variety of substrates with or without the heterogeneous catalysts Pt and RuO_2.[98,181,184] A number of these photocatalytic reactions and their mechanisms have been investigated.[11−15,185] The structures of the protonated 1.5-electron- and 1.8-electron-reduced anions are not significantly different from the structure of the oxidized anion.[186] $[NH_2Pr^i_2]_4[H_{1.5}W_{10}O_{32}]\cdot 8H_2O$, which consists of a 1:1 molar mixture of the one-electron-reduced species $[H_5O_2][NH_2Pr^i_2]_4[W_{10}O_{32}]\cdot 6H_2O$ and the diamagnetic two-electron-reduced species $[H_5O_2]_2[NH_2Pr^i_2]_4[W_{10}O_{32}]\cdot 4H_2O$, provides a single-crystal ESR spectrum showing the superhyperfine interaction due to eight magnetically equivalent ^1H atoms with an intensity ratio of 1:8:28:56:70:56:28:8:1 at 77 K. In $[NH_2Pr^i_2]_4[H_{1.5}W_{10}O_{32}]\cdot 8H_2O$, the terminal oxygen atom at each of the eight equatorial WO_6 sites is in contact with a water molecule which is hydrogen bonded in the lattice. Therefore, at 77 K the anion's paramagnetic electron is delocalized over the central four sets of two WO_6 octahedra linked through an axial μ-oxygen atom in a mode similar to what was seen with $[Mo_{14}O_{46}]^{10-}$. The interaction of the paramagnetic electron with the eight protons on the terminal oxygen atoms is due to the direct spin

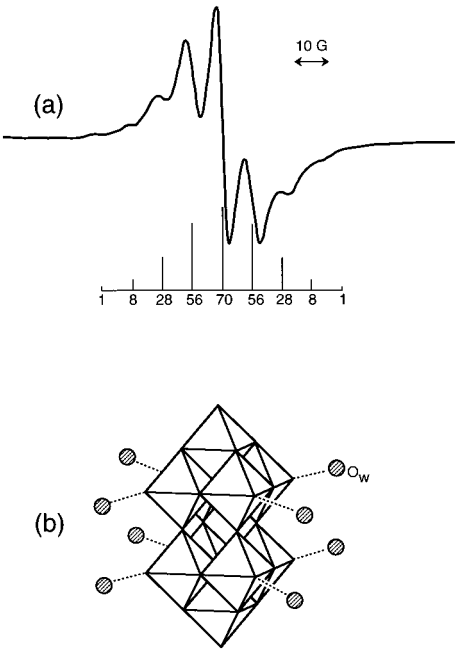

Figure 14. ESR spectrum (a) of $[NH_2Pr^i_2]_4[H_{1.5}W_{10}O_{32}]\cdot 8H_2O$ single crystal at 77 K and hydrogen bonds (b) among the terminal oxygen atoms at equatorial octahedral sites and lattice water molecules. The ESR signal indicates $g = 1.833$ and $A_H = 8.0$ G.

Table 6. Thermal Activation Energies for Electron-Hopping in the One-Electron-Reduced Polyoxometalates

compounds	E_{th}
$[W_6O_{19}]^{3-}$	0.055[95]
$[W_5NbO_{19}]^{4-}$	0.075[95]
$[H_2W_{12}O_{40}]^{7-}$	0.035[95]
$[SiW_{12}O_{40}]^{5-}$	0.035[95]
$[As_2W_{18}O_{62}]^{7-}$	0.040[95]
$[AsH_2W_{18}O_{60}]^{8-}$	0.040[95]
$[BW_{12}O_{40}]^{6-}$	0.004[96]
$[W_{10}O_{32}]^{5-}$	0.06[98,182]
$[Mo_6O_{19}]^{3-}$	0.155[94]
α-$[PMo_{12}O_{40}]^{4-}$	0.035[94]
α-$[GeMo_{12}O_{40}]^{5-}$	0.045[94]
β-$[SiMo_3W_9O_{40}]^{5-}$	0.055[94]
$[S_2Mo_{18}O_{62}]^{5-}$	0.0045 and 0.087[189]

polarization of the isopolyoxomolybdate lattice.[187] Figure 14 shows a typical ESR spectrum of $[NH_2Pr^i_2]_4[H_{1.5}W_{10}O_{32}]\cdot 8H_2O$ at 77 K along with the hydrogen bonds between the terminal oxygen atoms on the equatorial WO_6 octahedra and the water molecules in the lattice. ^{183}W NMR spectra of the two-electron-reduced species $[W_{10}O_{32}]^{6-}$ in various solutions indicate that the two electrons are delocalized primarily over the eight equatorial WO_6 octahedral sites.[98,182,188] A hopping process between the equatorial and axial WO_6 octahedra in the anion probably occurs in the protonated species $[H_2W_{10}O_{32}]^{4-}$, since the thermal activation energy (0.06 eV at >100 K) of the paramagnetic electron for the species $[HW_{10}O_{32}]^{4-}$ [98] is close to the value for $[W_6O_{19}]^{3-}$.[95] The thermal activation energies (E_{th}) estimated from Arrhenius plots of the observed ESR peak-to-peak line widths for the one-electron-reduced polyoxometalates in solution are listed in Table 6. The E_{th} = 0.0045 eV observed for the Dawson structure molybdosulfate $[S_2Mo_{18}O_{62}]^{5-}$ in the low-temperature

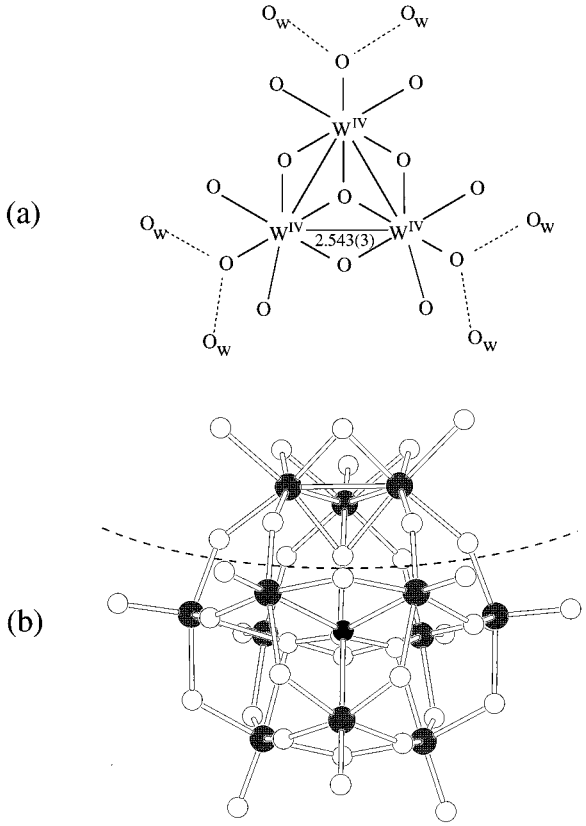

Figure 15. $W^{IV}_3O_{13}$ triad (a) and anion (b) structures of $[BW_{12}O_{37}(H_2O)_3]^{5-}$. Average $W^{IV}\cdots W^{IV}$ distance is denoted in Å.

range is ascribed to hopping over the whole anion lattice. This is based on the observation of 91 lines due to the coupling with 18 magnetically equivalent Mo nuclei (coupling constant ~4 G). Also, the E_{th} = 0.087 in the high-temperature range corresponds to an intermolecular hopping process.[189] This is in contrast to E_{th} = 0.155 and 0.075 eV observed for the intramolecular hopping in $[Mo_6O_{19}]^{3-}$ and $[W_5NbO_{19}]^{4-}$.[94,95]

Electron delocalization occurs over the whole W−O framework of the α-Keggin polyoxotungstate of two-electron-reduced $[Co^{II}W_{12}O_{40}]^{8-}$, which is prepared by electrolysis, and can be seen with a help of ^{183}W NMR spectroscopy.[190] $[H_2W_{12}O_{40}]^{6-}$, $[BW_{12}O_{40}]^{5-}$, and $[SiW_{12}O_{40}]^{4-}$ each can be reduced electrochemically, or photochemically in the case of $[BW_{12}O_{40}]^{5-}$, to a brown, six-electron-reduced species which is different from one- or two-electron-reduced species used as a precursor and which has a framework nearly identical to that of the oxidized species. ^{183}W NMR spectroscopy of the brown species indicates that six electrons are localized at the edge-shared $W^{IV}_3O_{13}$ triad where the terminal oxygen atoms are doubly protonated to form water molecules.[98,191−195] Although the first crystallographic study of the brown species was carried out on electrochemically formed $Rb_4H_8[H_2W^{IV}_3W^{VI}_9O_{40}]\cdot\sim 18H_2O$, the location of the $W^{IV}_3O_{13}$ group in the anion was uncertain due to orientational disorder of the crystal.[196] However, a perfect structure of the six-electron-reduced from was obtained for $K_5[BW_{12}O_{37}(H_2O)_3]\cdot 13.5H_2O$.[197] Figure 15 shows the structure of the α-form of the $[BW_{12}O_{37}(H_2O)_3]^{5-}$ anion. The photolysis of aqueous

solutions containing α-$[BW_{12}O_{40}]^{5-}$ and MeOH at pH < 2 led to the formation of the diamagnetic brown species $K_5[BW_{12}O_{37}(H_2O)_3]\cdot 13.5H_2O$ via successive disproportionations between the protonated two-electron-reduced species $[H_2BW_{12}O_{40}]^{5-}$.[96] The edge-shared W^{IV}_3 triad contains terminal aqua ligands. Each W^{IV} atom is bound to an aqua ligand with a mean bond length of 2.15 Å and is linked to other W^{IV} atoms by $W^{IV}-W^{IV}$ bonds (mean 2.543 Å). The aqua ligand is also bound to lattice water and to neighboring anion oxygen atoms via hydrogen bonds.

C. Polyoxovanadates and Self-Assembly Encapsulation

$[HV_2O_7]^{3-}$, which is in equilibrium with $[V_4O_{12}]^{4-}$ in basic media,[198,199] is photosensitive and acts as a photocatalyst for H_2 formation from electron-donating organic substances.[200] These vanadate species undergo photochemical self-assembly in the presence of small, negatively-charged or neutral species which act as templates, to yield a spherical cluster encapsulated by smaller species.[109,201,202] This photochemical encapsulation method allows the preparation processes to be easily controlled and provides many opportunities to make mixed-valence isomers which are different from the traditional compounds obtained by Müller and others.[203−208] Prolonged photolysis of aqueous solutions containing $[V_4O_{12}]^{4-}$ and MeOH at pH 9.5 in the presence of CO_3^{2-}, Cl^-, N_3^-, and PO_4^{3-} leads to the formation of $[V_{15}O_{36}(CO_3)]^{7-}$, $[V_{18}O_{42}(Cl)]^{13-}$, $[V_{18}O_{44}(N_3)]^{14-}$, and $[V_{18}O_{42}(PO_4)]^{11-}$ which have approximate symmetries of D_{3h}, D_{4d}, D_{2h}, and T_d, respectively. The shape of the anion clusters and the size of their central cavity (6−8 Å) strongly depend on the electrostatic interaction with templates. Most of the clusters consist of VO_5 square pyramids, to which additional VO_6 octahedra are connected in $[V_{15}O_{36}(CO_3)]^{7-}$ and $[V_{18}O_{42}(PO_4)]^{11-}$. The species $[V_{18}O_{42}(H_2O)]^{12-}$, which encapsulates a neutral water molecule, can be isolated as $K_{10}[H_2V_{18}O_{42}(H_2O)]\cdot 16H_2O$ from the photolysis of aqueous solutions of the $[V_4O_{12}]^{4-}$/MeOH/KOH system at pH 13.5. Figure 16 shows structures of these spherical anion clusters.

The sodium cation encapsulation species $[V_{12}B_{32}O_{84}(Na_4)]^{15-}$ is isolated as $H_7[V_{12}B_{32}O_{76}(OH)_8(Na)_4]\cdot 13H_2O$ from the photolysis of the $[V_4O_{12}]^{4-}$/MeOH/Na_3BO_3 system.[202] $[V_{12}B_{32}O_{76}(OH)_8(Na_4)]^{7-}$ consists of an edge-shared $(VO)_{12}O_{24}$ ring array of VO_5 square-pyramids, sandwiched between two $B_{16}O_{20}(OH)_4$ rings to form a cyclic doughnut-shaped framework. The central cavity of the cyclic anion is occupied by Na^+ cations. In $H_7[V_{12}B_{32}O_{76}(OH)_8(Na_4)]\cdot 13H_2O$, eight Na atoms (with approximate sizes of 2.62 × 2.62 × 2.98 Å) have been refined at the tetragonal corners with half occupancies due to disorder. This has resulted in the location of four Na^+ cations in an approximately tetrahedral arrangement with Na···Na distances of 3.69 and 3.99 Å. Figure 17 shows a representation of the structure of $[V_{12}B_{32}O_{76}(OH)_8(Na)_4]^{7-}$. Part of the Na^+ cations are accessible to exchange with trivalent lanthanide cations Ln^{3+}. Other cation (Li^+ or K^+)-encapsulated species have been prepared by a modified procedure.

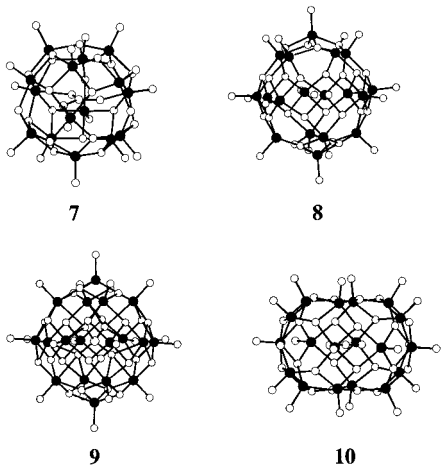

Figure 16. Structures of spherical cluster anions produced by photoinduced self-assembly encapsulation: $[V_{15}O_{36}(CO_3)]^{7-}$ (**7**), $[V_{18}O_{42}(Cl)]^{13-}$ (**8**), $[V_{18}O_{44}(N_3)]^{14-}$ (**9**), and $[V_{18}O_{42}(PO_4)]^{11-}$ (**10**).

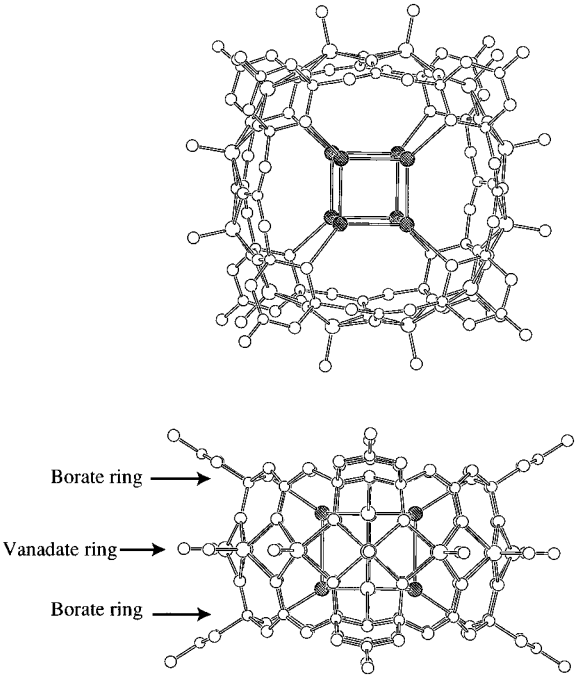

Figure 17. Schematic representation of the structure of $[V_{12}B_{32}O_{84}(Na_4)]^{15-}$. Eight Na atoms at the tetragonal corners are in half-occupancies.

Alkaline-metal-cation-encapsulated clusters also have been characterized for the polyoxotungstates $[Sb_9W_{21}O_{86}(Na)]^{18-}$,[209] $[As_4W_{40}O_{140}(K)]^{8-}$,[210] $[W_{18}O_{56}(HF_3)_2(Na)]^{7-}$,[211] and $[P_5W_{30}O_{110}(Na)]^{14-}$.[145] Another type of oxovanadium/borate cluster $(enH_2)_5[V_{12}B_{18}O_{54}(OH)_6]\cdot H_2O$ (en = ethylenediamine), in which the anion consists of a puckered $B_{18}O_{36}(OH)_6$ ring sandwiched between two triangles of six edge-shared vanadium atoms without any feasibility of encapsulation, can be hydrothermally synthesized at 170 °C in water.[212]

Chemically induced dynamic electron polarization (CIDEP) spectroscopy of the polyoxometalate/alcohol systems reveals that the precursor in the photoredox reaction of the polyoxometalates has O→M LMCT triplet states which abstract a hydrogen from an alcohol to yield a singly protonated polyoxometa-

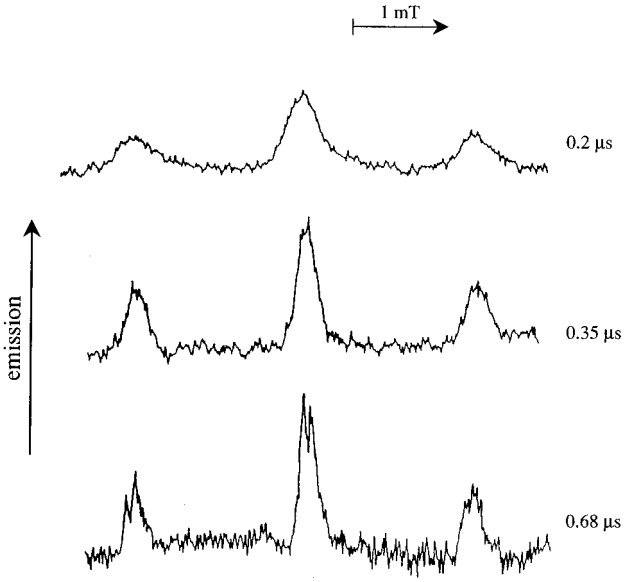

Figure 18. Time-resolved ESR spectra (at $g = 2.001$) taken at the delay times indicated during the photolysis of the $[V_4O_{12}]^{4-}$/MeOH at pH 9 at room temperature.

late and an α-hydroxyalkyl radical.[109] Figure 18 shows the CIDEP spectra at selected time delays following laser excitation of the $[V_4O_{12}]^{4-}$/MeOH system. The observed spectra at $g = 2.001$ show 1:2:1 triplet hyperfine structures (with an equal splitting of $A_{\alpha\text{-H}} = 1.76 \pm 0.03$ mT) due to the $^{\bullet}CH_2OH$ radical. The spectra also shows total emissive CIDEP signals within the first 2 μs after the laser pulse. Neither distortion of the ESR polarization of the $^{\bullet}CH_2OH$ radical nor the effect of an external magnetic field on the polarization can explain the triplet mechanism. The lifetime of the O→M LMCT triplet states at room temperature in aqueous solution should be much shorter than 100 μs (which is close to their lifetime at 100 K in the solid state), as shown in Table 5. The decay rate of the polarization of the $^{\bullet}CH_2OH$ radical by $[V_4O_{12}]^{4-}$ in water is estimated to be approximately $(0.9\ \mu s)^{-1}$, as shown in Figure 18. A similar result has been obtained for $[Mo_7O_{24}]^{6-}$ and $[W_{10}O_{32}]^{4-}$. Since the decay of the spin polarization of $^{\bullet}CH_2OH$ is close to the electron spin relaxation time (0.6 μs) of a $^{\bullet}CH_2OH$ radical generated by pulse radiolysis of a N_2O-saturated aqueous methanolic solution at pH 7,[213] the electron spin relaxation of the α-hydroxyalkyl radical must be a main process which terminates the polarization in the system. Little contribution from the one-electron-reduced species $[V_4O_{12}H]^{4-}$ to the time-resolved spectrum is observed, which indicates that the spin−lattice relaxation of the $[V_4O_{12}H]^{4-}$ is faster than that of the α-hydroxyalkyl radical. As discussed in section V.B. above, the energy transfer in the polyoxometalate lattices occurs via O→M LMCT triplet states. Therefore, the O→M LMCT triplet states participate in both electron-transfer and energy-transfer processes in the polyoxometalate lattices.

VII. Conclusions

The photochromic or electrochromic coloration of polyoxometalate and related metal oxide lattices occurs due to the trapping of d^1 electrons at appropriate metal sites (usually octahedral MO_6 sites) which results from photoexcitation of O→M LMCT bands or from electrochemical reduction. The trapped d^1 electrons cause visible light to be absorbed at d−d and/or intervalence charge-transfer bands. In photoinduced coloration, the holes, which are counter carriers, are trapped at a metastable site in the lattice. Without this trapping mechanism, the recombination of the electron and hole predominates, as exemplified by alkylammonium polyoxomolybdate lattices. Both electron transfers and energy transfers relevant to the relaxation of the O→M LMCT excited states in the polyoxometalate lattices are described. The intramolecular, d^1 electron transfer which occurs in both alkylammonium polyoxomolybdate and heteropoly blue lattices is discussed with regards to their crystal structures, and the intramolecular transfer to the O→M LMCT excitation energy is discussed in light of the photoluminescence spectroscopy results for the polyoxometalate lattices. The O→M LMCT triplet states are involved in both electron- and energy-transfer processes, and their relaxation is strongly associated with the magnitude of the electronic configuration disparities between the excited and ground states. Figure 19 shows the energy scheme for the photoinduced electron- and energy-transfer processes in addition to the electrochromism based on the electrochemical reduction and oxidation in the polyoxometalate lattice. The photoinduced self-assembly reaction which forms charged and neutral species encapsulated polyoxovanadate clusters is also described in terms of the photochemical construction of supramolecules.

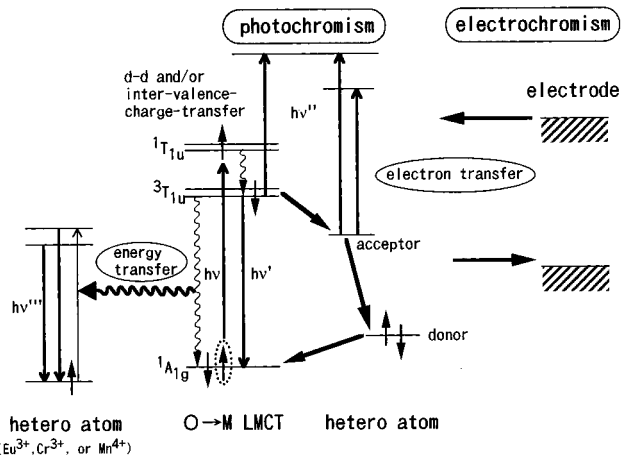

Figure 19. Energy scheme of photoinduced electron- and energy-transfer processes and electrochromism for the polyoxometalate lattices.

In order to achieve optical memory materials, it is necessary to find photochromic polyoxometalates in which the d^1 electron trapped at the lattice can be optically, rather than thermally, converted back to its original state with a high response time (of microsecond order at least). Unfortunately, few polyoxometalates exhibit both perfectly reversible photochromism and electrochromism. However, the solid-state photochemistry of polyoxometalates constitutes a valuable base for materials science, because it strongly contributes to the understanding of the

molecular level photochemistry and photophysics of nonmolecular metal oxide solids. The borders between these two fields are slowly fading, and the general features of polyoxometalate photochemistry, will be essential to constructing molecular devices as well as photochemically designing nanocomposites.

VIII. Acknowledgments

I acknowledge Grants-in-Aid for Scientific Research, No. 06241104 (for "Priority Area, New Development of Rare Earth Complexes"), No. 06403011, and No. 09354009 from the Ministry of Education, Science, Sports, and Culture for support of this work.

IX. References

(1) Rindel, M. S. *African J. Sci.* **1916**, *11*, 362.
(2) Sheppard, S. E.; Eberlin, L. W. U.S. Patent 1,934,451, 1933.
(3) Chalkley, L. *J. Phys. Chem.* **1952**, *56*, 1084.
(4) Chalkley, L. *J. Opt. Sci. Am.* **1954**, *44*, 699.
(5) Vogel, A. I. *A Text Book of Quantitative Inorganic Analysis*; Wiley and Sons: New York, 1966.
(6) Wu, H. *J. Biol. Chem.* **1920**, *43*, 189.
(7) Baudisch, O.; Gates, F. L. *J. Am. Chem. Soc.* **1934**, *56*, 373.
(8) Yamase, T.; Ikawa, T.; Kokado, H.; Inoue, E. *Chem. Lett.* **1973**, 615.
(9) Arnaud-Neu, F.; Schwing-Weill, M.-J. *Bull. Soc. Chim. Fr.* **1973**, 3225.
(10) Yamase, T.; Uheda, K. *J. Electrochem. Soc.* **1993**, *140*, 2378.
(11) Yamase, T. *Yuki Gosei Kyokaishi* **1985**, *43*, 249.
(12) Papaconstantinou, E. *Chem. Soc. Rev.* **1989**, *18*, 1.
(13) Yamase, T. In *Polyoxometalate Chemistry (Japanese)*; Kudo, T., Okuhara, T., Matsumoto, K., Yamase, T., Eds.; Kikan, Kagaku Sosetsu No. 20; Gakkai, Shuppan Center: Tokyo; 1993; p 92.
(14) Hill, C. L.; Prosser-McCartha, C. M. In *Photosensitization and Photocatalysis Using Inorganic and Organometallic Compounds*; Kalyanasundaram, K., Grätzel, M., Eds.; Kluwer Academic Publishers: Dordrecht, The Netherlands, 1993; p 307.
(15) Hill, C. L.; Kozik, M.; Winkler, J.; Hou, Y.; Prosser-McCartha, C. M. In *Photosensitive Metal-organic Systems: Mechanistic Principles and Applications*; Kutal, C., Serpone, N., Eds.; ACS Advances in Chemistry Series No. 238; American Chemical Society: Washington, DC, 1993; p 243.
(16) Deb, S. K.; Forrestal, J. L. *Photochromism*; Brown, G. H., Ed.; Wiley: New York, 1971; p 342.
(17) Faughnan, B. W.; Staebler, D. L.; Kiss, Z. T. In *Applied Solid States Science*: Wolke, R., Ed.; Academic Press: New York, 1971; p 107.
(18) Exelby, R.; Grinten, R. *Chem. Rev.* **1965**, *65*, 247.
(19) Faughnan, B. W.; Crandall, R. S.; Heyman, R. P. *RCA Rev.* **1975**, *36*, 177.
(20) Medved, D. B. *Am. Mineralogist* **1954**, *39*, 615.
(21) Kirk, R. D. *J. Electrochem. Soc.* **1954**, *101*, 461.
(22) Hodgson, W. G.; Brinen, J. S.; Williams, E. F. *J. Chem. Phys.* **1967**, *47*, 3719.
(23) Williams, E. F.; Hodgson, W. G.; Brinen, J. S. *J. Am. Ceram. Soc.* **1969**, *52*, 139.
(24) Ballentyne, D. W. G.; Bye, K. L. *J. Phys. D. Appl. Phys.* **1970**, *3*, 1438.
(25) Phillips, W. *J. Electrochem. Soc.* **1970**, *117*, 1557.
(26) McLaughlan, S. D.; Marshall, D. J. *J. Phys. Chem.* **1970**, *74*, 1359.
(27) Duncan, R. C.; Faughnan, B. W.; Phillips, W. *Appl. Opt.* **1970**, *9*, 2236.
(28) Schipper, D. J.; Van Doorn, C. Z.; Bolwijin, P. T. *J. Am. Ceram. Soc.* **1972**, *55*, 256.
(29) Doorn, C. Z.; Schipper, D. J.; Bolwijin, P. T. *J. Electrochem. Soc.* **1972**, *119*, 85.
(30) Bolwijin, P. T.; Schipper, D. J.; Van Doorn, C. Z. *J. Appl. Phys.* **1972**, *43*, 132.
(31) Heyman, P. M.; Gorog, I.; Faughnan, B. W. *IEEE Trans. Electron Devices* **1971**, *ED−18*, 685.
(32) Taylor, M. J.; Marshall, D. J.; Forrester, P. A.; McLaughlan, S. D. *Radio Eng. Electron.* **1970**, *40*, 17.
(33) Phillips, W.; Kiss, Z. *J. Proc. IEEE Lett.* **1968**, *56*, 2072.
(34) Faughnan, B. W.; Shidlovsky, I. *RCA Rev.* **1972**, *33*, 273.
(35) Takada, T.; Watanabe, A. *J. Electrochem. Soc.* **1973**, *120*, 1414.
(36) Chen, F. S.; LaMacchia, J. T.; Fraser, D. B. *Appl. Phys. Lett.* **1968**, *13*, 223.
(37) Amodel, J. J. *RCA Rev.* **1971**, *32*, 185.
(38) Staebler, D. L.; Amodel, J. J. *J. Appl. Phys.* **1972**, *43*, 1042.
(39) Amodel, J. J.; Phillips, W.; Staebler, D. L. *IEEE J. Quantum Electron.* **1971**, *QE-7*, 63.
(40) Staebler, D. L.; Phillips, W. *Appl. Phys. Lett.* **1974**, *24*, 268.
(41) Staebler, D. L.; Phillips, W. *Appl. Opt.* **1974**, *13*, 788.
(42) Staebler, D. L.; Burke, W. J.; Phillips, W.; Amodel, J. *J. Appl. Phys. Lett.* **1975**, *26*, 182.
(43) Parmelee, C. W.; Badger, A. *J. Am. Chem. Soc.* **1934**, *17*, 1.
(44) McTaggart, F. K.; Bear, J. *J. Appl. Chem. (London)* **1955**, 643.
(45) Weyl, W. A.; Forland, T. *Ind. Eng. Chem.* **1950**, *42*, 257.
(46) Faughnan, B. W.; Kiss, Z. J. *Phys. Rev. Lett.* **1968**, *21*, 1331.
(47) Colton, R.; Guzman, A. M.; Rabalais, J. W. *Acc. Chem. Rev.* **1978**, *11*, 170.
(48) Sakka, S. *J. Am. Ceram. Soc.* **1969**, *52*, 69.
(49) Deb, S. K. *Appl. Opt. Suppl.* **1969**, *3*, 192.
(50) Schoot, C. J.; Ponjee, J. J.; van Dam, H. T.; van Doorn, R. A.; Bolwijn, P. T. *Appl. Phys. Lett.* **1973**, *23*, 64.
(51) McIntyre, J. D. E.; Beni, G.; Shay, J. L. *Abstract of the 20th IEEE international Symposium on Electromagnetic Compatibility*; IEEE: Santa Barbara, CA, 1978.
(52) Nicholson, M. M.; Galiardi, R. V. *SID Digest.* **1978**, 24.
(53) Yoshiike, N.; Kondo, S.; Fukai, M. *J. Electrochem. Soc.* **1980**, *127*, 1496.
(54) Arnoldussen, T. C. *J. Electrochem. Soc.* **1981**, *128*, 117.
(55) Hurditch, R. *Electron. Lett.* **1975**, *11*, 142.
(56) Zeller, H. R.; Beyeller, H. V. *Appl. Phys.* **1977**, *13*, 231.
(57) Deneuville, A.; Gerard, P.; Billat, P. *Thin Solid Films* **1980**, *70*, 203.
(58) Hajimoto, Y.; Matsushita, M.; Ogura, S. *J. Electron. Mater.* **1979**, *8*, 301.
(59) Crandall, R. S.; Faughnan, B. W. *Appl. Phys. Lett.* **1976**, *28*, 95.
(60) Yoshiike, N.; Kondo, S. *J. Electrochem. Soc.* **1983**, *130*, 2283.
(61) Yoshiike, N.; Kondo, S. *J. Electrochem. Soc.* **1984**, *131*, 809.
(62) Yoshiike, N.; Ayusawa, M.; Kondo, S. *J. Electrochem. Soc.* **1984**, *131*, 2600.
(63) Reichman, B.; Bard, A. *J. Electrochem. Soc.* **1979**, *126*, 583.
(64) Ando, E.; Kawakami, K.; Matsuhiro, K.; Masuda, Y. *Displays* **1985**, 3.
(65) Zhang, J.-G.; Benson, D. K.; Tracy, C. E.; Deb, S. K.; Czanderna, A. W.; Crandall, R. S. *J. Electrochem. Soc.* **1994**, *141*, 2795.
(66) Mathew, J. G. H.; Sapers, S. P.; Cumbo, M. J.; O'Brien, N. A. In *Electrochromic Materials III*; Ho, K.-C., Greenberg, C. B., MacArthur, D. M., Eds.; Electrochemical Society Proceedings; Electrochemical Society, Inc.: Pennington, 1997; Vols. 96−24, p 311.
(67) Beni, G.; Shay, J. L. *Appl. Phys. Lett.* **1978**, *33*, 567.
(68) Shay, J. L.; Beni, G.; Schiavone, L. *Appl. Phys. Lett.* **1978**, *33*, 942.
(69) Gottesfeld, S.; McIntyre, J. D. E. *J. Electrochem. Soc.* **1979**, *126*, 742.
(70) Kang, K. S.; Shay, J. L. *J. Electrochem. Soc.* **1983**, *130*, 766.
(71) Sato, Y.; Ono, K.; Kobayashi, T.; Wakabayashi, H.; Yamanaka, H. *J. Electrochem. Soc.* **1987**, *134*, 570.
(72) Yu, P. C.; Nazri, G.; Lampert, C. M. *Solar Energy Mater.* **1987**, *16*, 1.
(73) Morisaki, S.; Kawakami, K.; Baba, N. *Jpn. J. Appl. Phys.* **1988**, *27*, 314.
(74) Granqvist, C. G. *Handbook, of Inorganic Electrochromic Materials*; Elsevier: Amsterdam, 1995.
(75) Decker, F.; Passerini, S.; Pileggi, R.; Scrosati, B. *Electrochim. Acta* **1994**, *37*, 1033.
(76) Lourenco, A.; Origo, F. D.; Gorenstein, A.; Passerini, S.; Smyrl, A. W. H.; Fantini, M. C. A.; Tabacniks, M. H. In *Electrochromic Materials III*; Ho, K.-C., Greenberg, C. B., MacArthur, D. M., Eds.; Electrochemical Society Proceedings; Electrochemical Society, Inc.: Pennington, 1997; Vols. 96−24, p 206.
(77) Yamase, T.; Hayashi, H.; Ikawa, T. *Chem. Lett.* **1974**, 1055.
(78) Yamase, T.; Ikawa, T. *Bull. Chem. Soc. Jpn.* **1977**, *50*, 746.
(79) Yamase, T. *J. Chem. Soc., Dalton Trans.* **1978**, 283.
(80) Arnaud-Neu, F.; Schwing-Weill, M.-J. *Bull. Soc. Chim. Fr.* **1973**, 3233.
(81) Ohasi, Y.; Yanagi, K.; Sasada, Y.; Yamase, T. *Bull. Chem. Soc. Jpn.* **1982**, *55*, 1254.
(82) Isobe, M.; Marumo, F.; Yamase, T.; Ikawa, T. *Acta Crystallogr.* **1978**, *B34*, 2728.
(83) Bharadwaj, P. K.; Ohashi, Y.; Sasada, Y.; Sasaki, Y.; Yamase, T. *Acta Crystallogr.* **1986**, *C42*, 545.
(84) Toraya, H.; Marumo, F.; Yamase, T. *Acta Crystallogr.* **1984**, *B40*, 145.
(85) Boeschen, F.; Buss, B.; Krebs, B. *Acta Crystallogr.* **1974**, *B30*, 48.
(86) Yamase, T.; Sugata, M.; Ishikawa, E. *Acta Crystallogr.* **1996**, *C52*, 1869.
(87) Yamase, T. *J. Chem. Soc., Dalton Trans.* **1982**, 1987.
(88) Yamase, T. *J. Chem. Soc., Dalton Trans.* **1985**, 2585.
(89) Yamase, T.; Suga, M. *J. Chem. Soc., Dalton Trans.* **1989**, 661.
(90) Pascaru, I.; Constantinescu, O.; Constantinescu, M.; Arigan, D. *Bull. Soc. Chim. Fr.* **1965**, 1283.
(91) Byfleet, C. R.; Hening, F. G.; Lin, W. C.; McDowell, C. A.; Ward, D. J. *Mol. Phys.* **1968**, *15*, 239.

(92) Atherton, N. M.; Blackford, R. D. S. *Mol. Phys.* **1987**, *61*, 443.
(93) Bharadwaj, P. K.; Ohashi, Y.; Sasada, Y.; Sasaki, Y.; Yamase, T. *Acta Crystallogr.* **1984**, *C40*, 48.
(94) Sanchez, C.; Livage, J. Launay, J. P.; Fournier, M.; Jeannin, Y. *J. Am. Chem. Soc.* **1982**, *104*, 3194.
(95) Sanchez, C.; Livage, J.; Launay, J. P.; Fournier, M. *J. Am. Chem. Soc.* **1983**, *105*, 6817.
(96) Yamase, T.; Watanabe, R. *J. Chem. Soc., Dalton Trans.* **1986**, 1669.
(97) Sasaki, Y.; Yamase T.; Ohashi, Y.; Sasada, Y. *Bull. Chem. Soc. Jpn.* **1987**, *60*, 4285.
(98) Yamase, T.; Usami, T. *J. Chem. Soc., Dalton Trans.* **1988**, 183.
(99) Prosser-McCartha, C. M.; Kadkhodayan, M.; Williamson, M. M.; Bouchard, D.; Hill, C. L. *J. Chem. Soc., Chem. Commun.* **1986**, 1747.
(100) Williamson, M. M.; Bouchard, D.; Hill, C. L. *Inorg. Chem.* **1987**, *26*, 1436.
(101) Hill, C. L.; Bouchard, D.; Kadkhodayan, M.; Williamson, M. M.; Schmidt, J. A.; Hilinski, E. F. *J. Am. Chem. Soc.* **1988**, *110*, 5471.
(102) Román, P.; Gutiérrez-Zorrilla, J. M.; Esteban-Calderón, C.; Martínez-Ripoll, M.; García-Blanco, S. *Polyhedron* **1985**, *4*, 1046.
(103) Román, P.; Gutiérrez-Zorrilla, J. M.; Martínez-Ripoll, M.; García-Blanco, S. *Polyhedron* **1986**, *5*, 1799.
(104) Román, P.; Gonzalez-Aguado, M. E.; Esteban-Calderón, C.; Martínez-Ripoll, M.; García-Blanco, S. *Z. Kristallogr.* **1983**, *165*, 271.
(105) Román, P.; Gutiérrez-Zorrilla, J. M.; Martínez-Ripoll, M.; García-Blanco, S. *J. Crystallogr. Spectrosc. Res.* **1987**, *17*, 109.
(106) Román, P.; Gutiérrez-Zorrilla, J. M.; Luque, A.; Martínez-Ripoll, M. *Z. Kristallogr.* **1988**, *184*, 175.
(107) Román, P.; Gutiérrez-Zorrilla, J. M.; Martínez-Ripoll, M. García-Blanco, S. *Z. Kristallogr.* **1985**, *173*, 169.
(108) Román, P.; San José, A.; Luque, A.; Gutiérrez-Zorrilla, J. M. *Inorg. Chem.* **1993**, *32*, 775.
(109) Yamase, T.; Ohtaka, K. *J. Chem. Soc., Dalton Trans.* **1994**, 2599.
(110) Adams, R.; Klemperer, W. G.; Liu, R.-S. *J. Chem. Soc., Chem. Commun.* **1979**, 256.
(111) McCarron, E. M., III; Harlow, R. L. *J. Am. Chem. Soc.* **1983**, *105*, 6179.
(112) McCarron, E. M., III; Whitney, J. F.; Chose, D. B. *Inorg. Chem.* **1984**, *23*, 3275.
(113) Kramenar, B.; Korpar-Colig, B.; Penavic, M.; Cindric, M. *J. Chem. Soc., Dalton Trans.* **1990**, *1125*.
(114) Inoue, M.; Yamase, T. *Bull. Chem. Soc. Jpn.* **1995**, *68*, 3055.
(115) Inoue, M.; Yamase, T. *Bull. Chem. Soc. Jpn.* **1996**, *69*, 2863.
(116) Attanasio, D.; Bonamico, M.; Fares, V.; Suber, L. *J. Chem. Soc., Dalton Trans.* **1992**, 2523.
(117) Tell, B.; Waguer, S. *Appl. Phys. Lett.* **1978**, *33*, 873.
(118) Tell, B.; Wudl, F. *J. Appl. Phys.* **1979**, *50*, 5944.
(119) Yamase, T.; Sasaki, Y.; Motowaki, T. *Inorg. Chim. Acta* **1986**, *121*, L19.
(120) Deschanvres, A.; Desgardin, G.; Raveau, B.; Thomazeau, J. C. *Bull. Soc. Chim. Fr.* **1967**, *12*, 4557.
(121) Yamase, T.; Matsuzawa, M.; Sasaki, Y. *Inorg. Chim. Acta* **1987**, *127*, L9.
(122) Kudo, T.; Okamoto, H.; Matsumoto, K.; Sasaki, Y. *Inorg. Chim. Acta* **1985**, *111*, L27.
(123) Kudo, T.; Kishimoto, A.; Takano, S.; Aikawa, Y. *Ohyo Butsuri* **1992**, *61*, 266.
(124) Stillman, M. J.; Thompson, A. J. *J. Chem. Soc., Dalton Trans.* **1976**, 1138.
(125) Blasse, G.; Dirksen, G. J.; Zonnevijlle, F. *J. Inorg. Nucl. Chem.* **1981**, *43*, 2847.
(126) Blasse, G.; Dirksen, G. J.; Zonnevijlle, F. *Chem. Phys. Lett.* **1981**, *83*, 449.
(127) Ballardini, R.; Mulazzani, Q. G.; Venturi, M.; Bolletta, F.; Balzani, V. *Inorg. Chem.* **1984**, *23*, 300.
(128) Ballardini, R.; Chiorboli, E.; Balzani, V. *Inorg. Chim. Acta* **1984**, *95*, 323.
(129) Darwent, J.; Flint, C. D.; O'Grady, P. J. *Chem. Phys. Lett.* **1986**, *127*, 547.
(130) Sugeta, M.; Yamase, T. *Bull. Chem. Soc. Jpn.* **1993**, *66*, 444.
(131) Yamase, T.; Naruke, H.; Sasaki, Y. J. *J. Chem. Soc., Dalton Trans.* **1990**, 1687.
(132) Yamase, T.; Naruke, H. *J. Chem. Soc., Dalton Trans.* **1991**, 285.
(133) Naruke, H.; Yamase, T. *J. Lumin.* **1991**, *50*, 55.
(134) Yamase, T.; Naruke, H. *Coord. Chem. Rev.* **1991**, *111*, 83.
(135) Yamase, T. In *Polyoxometalates: From Platonic Solids to Anti-Retroviral Activity*; Pope, M. T., Müller, A., Eds.; Kluwer Academic Publishers: Dordrecht, The Netherlands, 1994; p 337.
(136) Naruke, H.; Ozeki, T.; Yamase, T. *Acta Crystallogr.* **1991**, *C47*, 489.
(137) Ozeki, T.; Yamase, T.; Naruke, H.; Sasaki, Y. *Inorg. Chem.* **1994**, *33*, 409.
(138) Sugeta, M.; Yamase, T. *Acta Crystallgr.* **1997**, *C53*, 1166.
(139) Yamase, T.; Kobayashi, T.; Kettle, S. F. A. *J. Electrochem. Soc.* **1996**, *143*, 1678.
(140) Yamase, T.; Sugeta, M. *J. Chem. Soc., Dalton Trans.* **1993**, 759.
(141) Kraut, B.; Ferraudi, G. *Inorg. Chem.* **1990**, *29*, 4834.
(142) Ozeki, T.; Takahashi, M.; Yamase, T. *Acta Crystallogr.* **1992**, *C48*, 1370.
(143) Ozeki, T.; Yamase, T. *J. Alloys Compd.* **1993**, *192*, 28.
(144) Ibal, J.; Low, J. N.; Weakley, T. J. R. *J. Chem. Soc., Dalton Trans.* **1974**, 2021.
(145) Alizadeh, M. H.; Harmalker, S. P.; Jeannin, Y.; Martin-Frere, J.; Pope, M. T. *J. Am. Chem. Soc.* **1985**, *107*, 2662.
(146) Creaser, I.; Heckel, M. C.; Neitz, R. J.; Pope, M. T. *Inorg. Chem.* **1993**, *32*, 1573.
(147) Soderholm, L.; Liu, G. K.; Muntean, J.; Malinsky, J.; Antonio, M. R. *J. Phys. Chem.* **1995**, *99*, 9611.
(148) Yamase, Y.; Ozeki, T.; Sakamoto, H.; Nishiya, S.; Yamamoto, A. *Bull. Chem. Soc. Jpn.* **1993**, *66*, 103.
(149) Blasse, G. In *Handbook on the Physics and Chemistry of Rare-Earths*; Gschneider, K. A., Jr.; Eyring, L., Eds.; North-Holland: Amsterdam, 1979; p 237.
(150) Verweg, J. W. M.; Dirksen, G. J.; Blasse, G. *J. Non-Cryst. Solids* **1988**, *107*, 49.
(151) Yamase, T.; Kobayashi, T.; Sugeta, M.; Naruke, H. *J. Phys. Chem.* **1997**, *101*, 5046.
(152) Horrocks, W. D., Jr.; Sudnick, D. R. *Acc. Chem. Res.* **1981**, *14*, 384.
(153) Naruke, H.; Yamase, T. *Acta Crystallogr.* **1992**, *C48*, 597.
(154) van Oosterholt, A. B. *J. Chem. Phys.* **1977**, *67*, 2412.
(155) van Oosterholt, A. B. *Phys. Status. Solidi A* **1977**, *41*, 601.
(156) van der Poel, W. A. J. A.; Noort, M.; Herbich, J.; Coremans, C. J. M.; van der Waals, J. H. *Chem. Phys. Lett.* **1984**, *103*, 245.
(157) van der Poel, W. A. J. A.; Herbich, J.; van der Waals, J. H. *Chem. Phys. Lett.* **1984**, *104*, 253.
(158) Barendswaards, W.; Weber, R. T.; van der Waals, J. H. *J. Chem. Phys.* **1987**, *87*, 3731.
(159) Barendswaards, W.; van der Waals, J. H. *Mol. Phys.* **1986**, *59*, 337.
(160) Barendswaards, W.; van Tol, J.; Weber, R. T.; van der Waals, J. H. *Mol. Phys.* **1989**, *67*, 651.
(161) van Tol, J.; van Hulst, J. A.; van der Waals, J. H. *Mol. Phys.* **1992**, *76*, 547.
(162) van Tol, J.; van der Waals, J. H. *Mol. Phys.* **1992**, *76*, 567.
(163) Yamase, T.; Sasaki, R.; Ikawa, T. *J. Chem. Soc., Dalton Trans.* **1981**, 628.
(164) Yamase, T.; Ikawa, T. *Inorg. Chim. Acta* **1979**, *37*, L529.
(165) Yamase, T.; Ikawa, T. *Inorg. Chim. Acta* **1980**, *45*, L55.
(166) Yamase, T.; Kurozumi, T. *J. Chem. Soc., Dalton Trans.* **1983**, 2205.
(167) Ward, M.; Brazdil, J. F.; Grasselli, R. K. *J. Phys. Chem.* **1984**, *88*, 4210.
(168) Kraut, B.; Ferraudi, G. *Inorg. Chem.* **1989**, *28*, 2692.
(169) Kraut, B.; Ferraudi, G. *J. Chem. Soc., Dalton Trans.* **1991**, 2063.
(170) Yamase, T. *J. Chem. Soc., Dalton Trans.* **1991**, 3055.
(171) Proust, A.; Robert, F.; Gouzerh, P.; Chen, Q.; Zubieta, J. *J. Am. Chem. Soc.* **1997**, *119*, 3523.
(172) Müller, A.; Plass, W.; Krickemeyer, E.; Dillinger, S.; Bögge, H.; Armatage, A.; Proust, A.; Beugholt, C.; Bergmann, U. *Angew. Chem., Int. Ed. Engl.* **1994**, *33*, 849.
(173) Zhang, S.-W.; Wei, Y.-G.; Yu, Q.; Shao, M.-C.; Tang, Y.-Q. *J. Am. Chem. Soc.* **1997**, *119*, 6440.
(174) Müller, A.; Meyer, J.; Krickemeyer, E.; Diemann, E. *Angew. Chem., Int. Ed. Engl.* **1996**, *35*, 1206.
(175) Müller, A.; Krickemeyer, E.; Bögge, H.; Schmidtmann, M.; Peters, F.; Menke, C.; Meyer, J. *Angew. Chem., Int. Ed. Engl.* **1997**, *36*, 484.
(176) Müller, A.; Krickemeyer, E.; Penk, M.; Wittneben, V.; Döring, J. *Angew. Chem., Int. Ed. Engl.* **1990**, *29*, 88.
(177) Neier, R.; Trojanowski, C.; Mattes, R. *J. Chem. Soc., Dalton Trans.* **1995**, 2521.
(178) Barrows, J. M.; Jameson, G. B.; Pope, M. T. *J. Am. Chem. Soc.* **1985**, *107*, 1771.
(179) Termes, S. C.; Pope, M. T. *Inorg. Chem.* **1978**, *17*, 500.
(180) Boyer, M. J. *Electroanal. Chem. Interfacial Electrochem.* **1971**, *31*, 441.
(181) Yamase, T.; Takabayashi, N.; Kaji, M. *J. Chem. Soc., Dalton Trans.* **1984**, 793.
(182) Chemseddine, A.; Sanchez, C.; Livage, L.; Launay, J.-P.; Fournier, M. *Inorg. Chem.* **1984**, *23*, 2609.
(183) Yamase, T. *Inorg. Chim. Acta* **1981**, *54*, L165.
(184) Rennecke, R. F.; Kadkhodayan, M.; Pasquali, M.; Hill, C. L. *J. Am. Chem. Soc.* **1991**, *113*, 8357.
(185) Ermolenko, L. P.; Delaire, J. A.; Giannoti, C. *J. Chem. Soc., Perkin Trans. 2* **1997**, 25.
(186) Sasaki, Y.; Yamase, T.; Ohashi, Y.; Sasada, Y. *Bull. Chem. Soc. Jpn.* **1987**, *60*, 4285.
(187) Yamase, T. *J. Chem. Soc., Dalton Trans.* **1987**, 1597.
(188) Duncan, D. C.; Hill, C. L. *Inorg. Chem.* **1997**, *35*, 5828.
(189) Cooper, J. B.; Way, D. M.; Bond, A. M.; Wedd, A. G. *Inorg. Chem.* **1993**, *32*, 2416.
(190) Casan-Pastorn, N.; Gomez-Romero, P.; Jameson, G. B.; Baker, L. C. W. *J. Am. Chem. Soc.* **1991**, *113*, 5658.
(191) Launay, J. P. *J. Inorg. Nucl. Chem.* **1976**, *38*, 807.
(192) Kazanski, L. P.; Launay, J. P. *Chem. Phys. Lett.* **1977**, *51*, 242.

(193) Fruchart, J. M.; Hervé, G. *Ann. Chim. (Paris)* **1971**, *6*, 337.
(194) Piepgrass, K.; Pope, M. T. *J. Am. Chem. Soc.* **1987**, *109*, 1586.
(195) Piepgrass, K.; Pope, M. T. *J. Am. Chem. Soc.* **1989**, *111*, 753.
(196) Jeannin, Y.; Launay, J. P.; Seid Sedjadi, M. A. *Inorg. Chem.* **1980**, *19*, 2933.
(197) Yamase, T.; Ishikawa, E. *J. Chem. Soc., Dalton Trans.* **1996**, 1619.
(198) Rehder, D. *Bull. Magn. Reson.* **1982**, *4*, 33.
(199) Pettersson, L.; Hedman, B.; Anderson, I.; Ingri, N. *Chem. Scr.* **1983**, *22*, 254.
(200) Yamase, T.; Watanabe, R. *Inorg. Chim. Acta.* **1983**, *77*, L193.
(201) Yamase, T.; Ohtaka, K.; Suzuki, M. *J. Chem. Soc., Dalton Trans.* **1996**, 283.
(202) Yamase, T.; Suzuki, M.; Ohtaka, K. *J. Chem. Soc., Dalton Trans.* **1997**, 2463.
(203) Müller, A.; Krickemeyer, E.; Penk, M.; Walberg, H.-J.; Bögge, H. *Angew. Chem., Int. Ed. Engl.* **1987**, *26*, 1045.
(204) Pope, M. T.; Müller, A. *Angew. Chem., Int. Ed. Engl.* **1991**, *30*, 34.
(205) Müller, A.; Reuter, H.; Dillinger, S. *Angew. Chem., Int. Ed. Engl.* **1995**, *34*, 2328.
(206) Day, V. W.; Klemperer, W. G.; Yaghi, O. M. *J. Am. Chem. Soc.* **1989**, *111*, 5959.
(207) Chang, Y. D.; Salta, J.; Zubieta, J. *Angew. Chem., Int. Ed. Engl.* **1994**, *33*, 325.
(208) Suber, L.; Bonamico, M.; Fares, V. *Inorg. Chem.* **1997**, *36*, 2030.
(209) Fischer, J.; Ricard, L.; Weiss, R. *J. Am. Chem. Soc.* **1976**, *98*, 3050.
(210) Robert, F.; Leyrie, M.; Hervé, G.; Tézé, A.; Jeannin, Y. *Inorg. Chem.* **1980**, *19*, 1746.
(211) Jorris, T. L.; Kozik, M.; Baker, L. C. *Inorg. Chem.* **1990**, *29*, 1746.
(212) Fijssenbeek, J. T.; Rose, D. J.; Haushalter, R. C.; Zubieta, J. *Angew. Chem., Int. Ed. Engl.* **1997**, *36*, 1008.
(213) Bartels, D. M.; Lawler, R. G.; Trifanac, A. D. *J. Chem. Phys.* **1985**, *83*, 2686.

CR9604043